Energy Reports 9 (2023) 833–858

Contents lists available at ScienceDirect

Energy Reports

journal homepage: www.elsevier.com/locate/egyr

Review article

Low voltage ride through capability for resilient electrical distribution system integrated with renewable energy resources

Monika Yadav [a,b], Nitai Pal [a], Devender Kumar Saini [b,*]

[a] Department of Electrical Engineering, Indian Institute of Technology (Indian School of Mines), Dhanbad, India
[b] Electrical Cluster, School of Engineering, University of Petroleum & Energy studies, Dehradun, India

ARTICLE INFO

Article history:
Received 9 September 2022
Received in revised form 11 November 2022
Accepted 7 December 2022
Available online 15 December 2022

Dataset link: https://drive.google.com/drive/folders/1hjhM1VAgIcjZlsT0466AdV7y-quRNkQB?usp=sharing

Keywords:
Grid codes
Low voltage ride through fault (LVRT)
Distribution grid
Renewable energy sources (RES)
Resiliency

ABSTRACT

It is evident that renewable energy sources (RES), will soon be considered as primary energy source in electrical networks. However, the increased penetration of RES along with the variable charging profile of electric vehicles in the distribution grid will pose serious technical challenges such as network instability, protection malfunctioning, aggravated line, and low- and high-voltage ride through capabilities. Moreover, the frequent occurrence of natural disasters has posed different dimensional problems for distribution system engineers. Hence, owing to the immediate demand for resilient electrical systems, many researchers have presented planning and operating techniques for resiliency enhancement. Consequently, application of low-voltage ride through (LVRT) during grid transformation in small clusters has significant role. However, the implementation of LVRT in operational methods during the transformation of an electric grid after a natural disaster has a lean share in the literature. Moreover, the applicability of grid code during microgrid formation due to extreme events also drives the planning and operational methodology. Therefore, this article first substantiates the importance of grid codes and IEEE standards for the interconnection of RES plants into a grid. Additionally, the paper presents a succinct summary on various control strategies to overcome the challenges of fault ride through capability, reactive power support, and anti-islanding in integrated wind and solar plants. Thenceforth, the importance of LVRT visibility in resiliency enhancement validated by simulating the urban electrical grid using the DIgSILENT PowerFactory Software.

Contents

* Corresponding author.
E-mail address: dev.iit.roorkee@gmail.com (D.K. Saini).

https://doi.org/10.1016/j.egyr.2022.12.023

Nomenclature

Indices and sets

f	Frequency
P_{min}, P_{max}	Active Power Limits
Q_{min}, Q_{max}	Reactive Power Limits
t	Time
T_r	Recovery time
T_F	Time at which voltage drops due to Fault
V_{DER}	Voltage of Distributed energy resources
V_{AF}	Voltage after Fault
V_F	Voltage at the time of Fault
V_g	Voltage at grid
V_n	Nominal Voltage
V_{PCC}	Voltage at point of common coupling
L_c	Earthquake Location
σ	Standard deviation
μ	Mean
x	Random Variable
$F(x)$	Fragility function
E	Expected mean
M_{eh}	Earthquake magnitude
R	Radial distance between fault earthquake line and site

Abbreviations

CEA	Central Electricity Authority
DER	Distributed energy resources
DFIG	Doubly fed Induction Generator
DVR	Dynamic Voltage Restorer
EV	Electric Vehicle
FRT	Fault ride through
GOI	Government of India
HVRT	High Voltage Ride Through
IEC	International electrical commission
IWGC	Indian wind energy grid code
LVRT	Low Voltage Ride Through
PCC	Point of Common Coupling
PMSG	Permanent magnet synchronous generator
PR	Proportional resonant
PV	Photovoltaic
RCI	Reactive current injection
RE	Renewable Energy
RES	Renewable Energy Sources
SG	Synchronous Generator
SCIG	Squirrel Cage Induction Generator
SLDC	State Load Dispatch Centre
WPP	Wind Power Plant
WRSG	Wound Rotor Synchronous Generator
WRT	Wind Turbine Generator
WT	Wind Turbine
ZVRT	Zero voltage ride through
PDF	Probability distribution function

1. Introduction

The increase in world population, decline in coal reserves, influx of electric vehicles (EVs) into the grid and climate change have resulted in an exponential increase in power demand. Hence, switching to nonconventional energy resources becomes a necessity. Therefore, it is evident that the decline in coal leads to an increase in energy demand from renewable energy sources (RES), which was 15% in 2020 and will increase to 27% by 2050, U.S.D. of Energy (2021) and Venkateswaran et al. (2020) as shown in Fig. 1. In addition, the influx of EVs worldwide has also posed serious challenges to the distribution grid operators. Data loges, over 3.2 million electric vehicles sold in the year 2021 and expected more than 200 million till 2030 (Gonzalez Venegas et al., 2020). Moreover, the EVs charging system is creating congestion to the distribution grid especially in peak load hours. Therefore, the load and voltage stress become critically high on the low voltage distribution grid during peak hours. The inclusion of grid tied EVs infrastructure poses active power loss, phase unbalancing, overloading and voltage drop. However, these technical constraints vary as per EVs growth rate, topology of the distribution grid, and the load demand of the region. It necessitates, distribution operators to work on infrastructure reinforcement. Moreover, the infusion of distributed energy generations (DERs), along with RES and battery storage, will make distribution grid flexible and resilient to meet priority loads. In contrast, emulation of machine learning probabilistic approach in planning phase for paradigm shifting from conventional to non-conventional energy, saves billions, for power companies. Furthermore, with this approach, control on cyberattack, grid damage condition, prediction of load, and energy market scenario can be predicted (Ahmad et al., 2022). Also, integrated approaches like industrial artificial intelligence and edge computing can be implemented for restoration of smart grid after the fault (Lamnatou et al., 2022).

In addition, the occurrence of natural disaster (high impact low probability) events also become triple times due to rapid climate change, and raises concern for the grid operators (Yadav et al., 2021). Evidently, the highest turbulence of natural disaster received in the last decade (2010–2019), worldwide. Therefore, a resilient, flexible and stable grid that can stand against the natural disaster and able to tackle stochastic demand of EVs system is imperative to build. Table 1 (IIT Kanpur, 2001; Paul et al., 2018; Racy, 2012; India Raises Flood Death Toll To 5, 2013) shows some deadliest extreme events, that in turn creates the necessity of a robust and resilient power grid as the main concern in future prospects to face the extreme events.

Considering the frequency of occurrence of extreme events and their devastating impact over distribution grid as well as cost for reconstruction, call to put endeavour in developing the methodology and metrics for boosting the resilience of power network against extreme events. Though, this is quite challenging with few concerns:

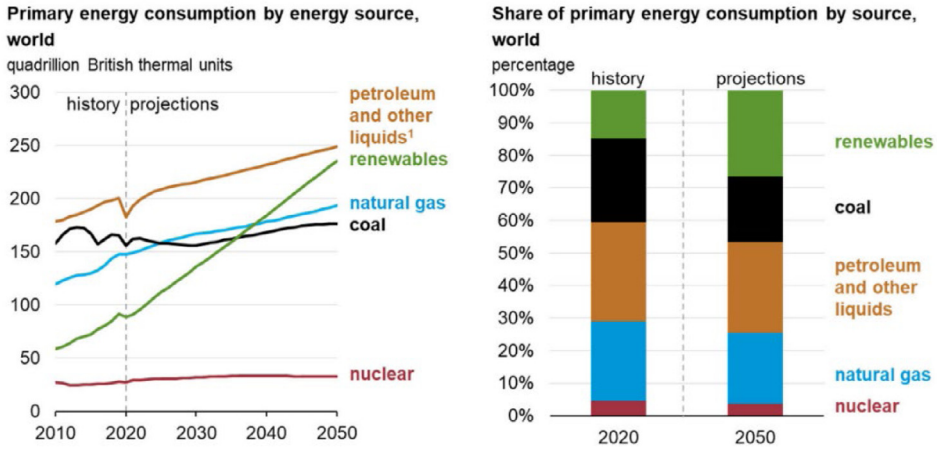

Fig. 1. Share of worldwide energy consumption (U.S.D. of Energy, 2021).

Table 1
Extreme events in India and worldwide.

Extreme events	Year	Outage period	Country/state	Remarks
Bhuj earthquake	January 2001	Few months	India	1. 7.7 magnitude 2. 13,805–20,023 dead; ∼166,800 injured Damage cost apprx. $7.5 billion
Indian ocean earthquake and tsunami	December 2004	Few months	India	1. Deadliest 2. 12,405 people lost their lives in India 3. 9.1 to 9.3 magnitude
Derecho Storm	June 2012	10 days	North american derecho	1. Deadliest storm 2. 4.2 million people faced outages in 11 states 3. Damage Cost: $2.9 billion
Hurricane Sandy	October 2012	09 days	U.S.	1. Deadliest hurricane 2. 9.3 million customers faced outages in 20 states 3. $68.7 billion (2012 USD)
Uttarakhand flash Flood (Kedarnath)	June 2013	2 months	India	1. Most disastrous 2. 5700 approx. people lost their lives. 3. 2052 houses wiped off 4. 147 bridges collapsed Rs 50,000 crore in damage cost
Kashmir Floods	September 2014	3 weeks	India	1. Reported 550+ no. of people lost their life 2. Rs. 5000 cr and 6000 cr. Damage cost
Hurricane Maria	September 2017	4 to 6 months in few areas	Puerto Rico	1. 3.6 million customers faced outages 2. $90 billion (2017 USD)
Hawaii earthquake	May 2018	3 to 6 days	Hawaii	1. 6.9 magnitude 2. 14,000 people faced outages
Cyclone Fani	May 2019	2 weeks	India	₹58 thousand crores damage cost

1. Expansion of distribution grid due to intense tapping of new loads makes it complex system.
2. No standard resilience metric and assessment is existing.

Resilience in field of power grid is quite new so there is notable requirement in terms of standard protocol and policy. In the context of power network, "resilience" terms have several aspects such as "absorb" and "recover" from a disastrous event. Author Panteli et al. (2016), presented a resilience definition in term with extreme weather events. "Resilience" can also be defined as "the grid's ability to withstand against the high-impact low-probability events that may have never been experienced before, able to rapidly recover from such disastrous events, and adapt its operation and structure to prevent or mitigate the impact of similar events in the future. Some structural attributes, defines and differentiate the resiliency aspect from reliability has sculpted in Fig. 2.

Recent studies have presented resiliency enhancement strategies by considering various disaster events such as typhoon, earthquake, flood, cyclone etc. For example, Ding et al. (2020) proposed a three-stage stochastic model for the resiliency enhancement during typhoon attack. Furthermore, the proposed model considered many factors for resiliency enhancement such as placement, structure reconfiguration, load recovery strategy, prediction of typhoon path with the anticipation scheme and validated the result on IEEE 33 and 144 bus system. In addition, Seongmun oh et al. proposed a multi-stage damage estimation methodology by taking 10 years cyclone, grid damage and weather historical data of south Korea (Oh et al., 2022). It is concluded that the grid resiliency enhancement lies in two dimensions: one is the operational strategies and another by infrastructure hardening (Sepúlveda-Mora and Hegedus, 2022). However, most studies are oriented toward operational solutions such as load recovery, formation of multi-microgrids, and self-healing after disturbance (Yadav et al., 2020; Ding et al., 2017; Gao et al., 2016). Whereas, few literature studies also suggest the vulnerability assessment for the critical infrastructure and uncertainty quantification, like Roberto Rocchetta proposed the resiliency enhancement of critical infrastructure (Rocchetta, 2022), for controlled islanding mode, during fault. However, the

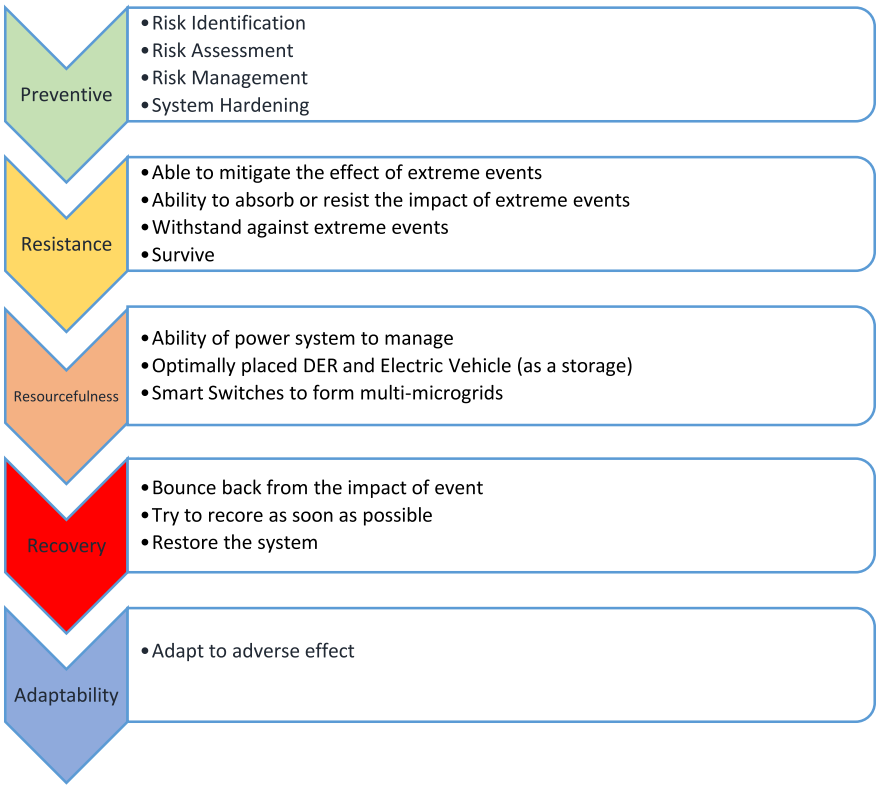

Fig. 2. Attributes required for power system resiliency.

applicability of infrastructure reinforcement founds limitation in developing countries, as it requires bulk capital investment, for re-structuring the entire electrical grid. Therefore, the probable solution that instead of restructuring the entire grid, hardening of the existing system is possible after finding vulnerable equipment using fragility curves (Golchoob Firoozjaee and Sheikh-El-Eslami, 2021; Yadav et al., 2021). In addition, the resiliency measurement during transition from grid to smart grid becomes imperative to validate the tools and techniques. Therefore, it has also been addressed in literature, for example resiliency measurement is reviewed in Das et al. (2020) and Younesi et al. (2022) and a case study on IEEE 33 system is conducted in two scenarios; one with the integrated PV units and another without PV units into the grid for the measurement of performance indices (Mishra et al., 2020).

The above-mentioned concern evident that inclusion of RES into the existing grid makes the system resilient but the constantly increasing number of RESs in the electrical grid also raises concerns about reliability, and stability. To address these concerns, operators regularly update the grid code and impose new regulations if required. Low-voltage ride through (LVRT) is a well-known requirement imposed by the operator for grid-connected RESs to maintain network stability (Zhao et al., 2017). It essentially requires, large RES plants remain connected during a fault or voltage sag/swell for a predefined time (Shabestary and Mohamed, 2020). This has also been addressed by Shabestary et al. by proposing a coordination control scheme for handling asymmetric LVRT to support grid stability (Shabestary and Mohamed, 2020). However, LVRT strategies vary based on connection and are categorized into two parts: one for independent renewable energy plants and the other for the grid-connected plant (Talha et al., 2020; Firouzi and Gharehpetian, 2018; Bahramian-Habil et al., 2021). For independent plants, RES get disconnected during the fault event as per protection strategies, whereas for the other one, various control strategies, either to support the voltage or to improve the LVRT capability, were proposed and presented in the studies (Gkavanoudis and Demoulias, 2015; Sadeghkhani et al., 2018).

The above discussion evident that, inconsiderable attentions have been paid to LVRT capability during the transition from grid to multi-microgrid. Apart from the planning and hardening phases, the integration of RESs on the distribution grid is mainly concerned with three problems during operation: LVRT, reactive power support, and anti-islanding (Pal and Panigrahi, 2020). Therefore, this study analyses control techniques used to overcome the aforementioned problems by considering disturbances. If any disturbance occurs in the grid system, disconnection of the RES is not possible, as it may leads to stability collapse. Moreover, the simultaneous disconnection of all RES sources leads to power outages. Therefore, this study substantiates the impact of LVRT in solar and wind power plants and validates its requirement by simulating an Indian urban electrical grid using the DIgSILENT PowerFactory software.

The remainder of this paper is organized as follows: Section 2 explains the grid code requirements for fault ride through, anti-islanding, and reactive current support. The working of various state logics for low-voltage ride through for generic/wind RESs are explained in Section 3, and for the solar power plant in Section 4. Section 5 illustrates the various control strategies used to enhance the fault ride through requirements for RES. Section 6 presents the need of LVRT implementation in resiliency enhancement using simulations. Sections 7 and 8 present brief discussions and conclusions, respectively.

2. Grid codes requirement

Grid codes are legal standards that provide technical requirements for integrating large RES plants to the transmission end to enhance system stability. Earlier, these requirements were usually issued by transmission system operators (Yadav et al., 2017) as RESs were installed at the transmission end only but

Table 2
Parameters and test instruments required for performance analysis.

Parameters to check	Test device	Remark
Voltage/current fluctuations	Grid simulation converter, digital oscilloscope	Range of voltage, current w.r.t. specified limit.
Power quality	Power quality monitoring device	To check the harmonics, voltage deviation.
LVRT	Grid fault simulator and power analyzer.	Overcome the voltage dip
HVRT	Grid fault simulator and power analyzer.	Overcome the voltage boost
Anti-islanding	Controlled DC source, anti-islanding test device and digital oscilloscope	Prevent RE plant to go in islanding
Inertial & damping control in wind plant	Grid simulation converter, digital oscilloscope	Vary the frequency of grid, and check the response
Black start capability test	–	Capability of plant to generate voltage without external supply and able to reconnect with grid.

now it is mandate document for the complete power network. Grid code compliance is mandatory for all generating sources to ensure system stability. The high share of RES, such as solar and wind, on the distribution side requires grid code upgradation. However, system operator authorities from all various countries issued multiple grid standards for grid-connected RESs for stable operation.

Moreover, grid codes vary region to region. The grid code for the transmission side mainly concentrates on the voltage fluctuation, active and reactive power limits, frequency fluctuations, and plant performance. In contrast, the distribution side focuses on limited issues such as the anti-islanding mode, power quality, and fault level (Hagh and Khalili, 2019). In addition, system operators play a key role in evaluating the impact of multiple power plant operations. To analyse the impact, certain testing, alteration, and performance tests under different conditions were carried out (Yongning et al., 2019). In RES integrated plants, testing includes voltage/current fluctuations, power quality, low-voltage ride through (LVRT), high-voltage ride through (HVRT), reactive power variation, and anti-islanding mode protection to verify the potential of RES plants with grid compliance. Table 2 lists the parameters versus test instruments required for the performance analysis (Yongning et al., 2019).

Factually, solar PV plant deployment has increased exponentially due to their potential benefits such as low carbon emission, low cost for generation, sharing load of the grid and many more. On the other end, solar plant creates fluctuation in voltage, protection issues, reactive power losses and power quality issues. Hence, system operators are issuing and frequently improving the grid codes to minimize the negative impact of solar PV on the grid.

Therefore, the integration of RES must compliance the standards mentioned by IEEE 1547. The IEEE 1547 document mentioned mandatory criteria or technical requirement related to RESs performance, safety, testing, operation and maintenance. For example, IEEE 1547-2003 has 59.3 Hz under-frequency protection setting and 60.5 Hz over-frequency disconnection, which can poses a high risk of system stability (Basso, 2014; Rebollal et al., 2021; Kekatos et al., 2015). Fig. 2 Fig. 3 systematically presents the revised IEEE standards.

2.1. Fault ride through capability

The most frequent type of fault is line to ground (L–G) across the world for overhead lines. Moreover, various type of faults in grid connected PV systems also hamper the stability of entire power system (Saad et al., 2016). In addition, owing to the switching of the capacitor bank or an L–G fault, a rise in voltage occurs, known as a voltage swell. The fault ride through (FRT) capability in distribution grid defines the requirement for grid connected RES. The defined requirement is that all RES should remain connected for a short period during low sag. The FRT capability behaviour depends on the time variation w.r.t. voltage or frequency. Therefore, it is concluded that the FRT requirement is a curve expressed in terms of voltage versus time and frequency versus time (Hagh and Khalili, 2019). The FRT requirement is essential for the coordinated operation of protection devices by providing an optimized setting.

Overall, FRT covers three types of requirements: low-voltage ride through (LVRT), zero-voltage ride through (ZVRT), and high-voltage ride through (HVRT). FRT describes the dynamic requirement on the extent at which renewable sources can remain connected to the main grid and support the grid by supplying power during fault condition. Therefore, it is highly recommended to set rules for LVRT and HVRT during voltage sag and swell, respectively (ES-AENOR, 2009; BDEW, 2007; E.on Netz, 2006; Western Electricity Coordination Council (WECC), 2005), while ZVRT is a crucial case of LVRT, in which the voltage reaches zero at the time of fault (Benyamina et al., 2021). However, the author in Hagh and Khalili (2019) considered some FRT characteristics, such as short-circuit characteristics, network design, protection system, generator, and fault impedance.

The temporary faults are frequent and create inescapable variations in voltage, current, and frequency. Moreover, a resilient distribution grid to fulfil critical loads during natural disasters must undergo a transformation from one to several clustered grids (Yadav et al., 2021). Therefore, during disaster or temporary faults, operators should prefer the sources to stay connected for a defined duration to avoid unnecessary power loss (Hagh and Khalili, 2019) in clustered grid. However, earlier literature suggests that at the time of fault in the grid zone, RES preferred to disconnected from the main grid for protection purposes, as voltage fluctuations will affect RES, such as the sudden increase in rotor speed in the wind system (Lokesh et al., 2021). Conversely, in 2003, E. ON, a European electric utility company issued the FRT requirements that at the time of fault, the wind sources should ride through in the following conditions (Ding et al., 2017):

i. The voltage at the grid (V_g) falls below 0.9 p.u. i.e. 90% of the rated value.
ii. The voltage at grid is in the range of ZVRT $>$ V_g $>$ HVRT limit line.

Furthermore, the RES are supposed to be disconnect if the voltage level has not reached 0.9 p.u. of the rated value after 1500 ms. Fig. 4(a) shows the FRT requirements issued by E. ON whereas Fig. 4(b) shows the FRT requirements followed by different countries (Ding et al., 2017).

In 2013, the Central Electricity Authority (CEA) updated the grid code by issued the “connectivity standards” for integrated

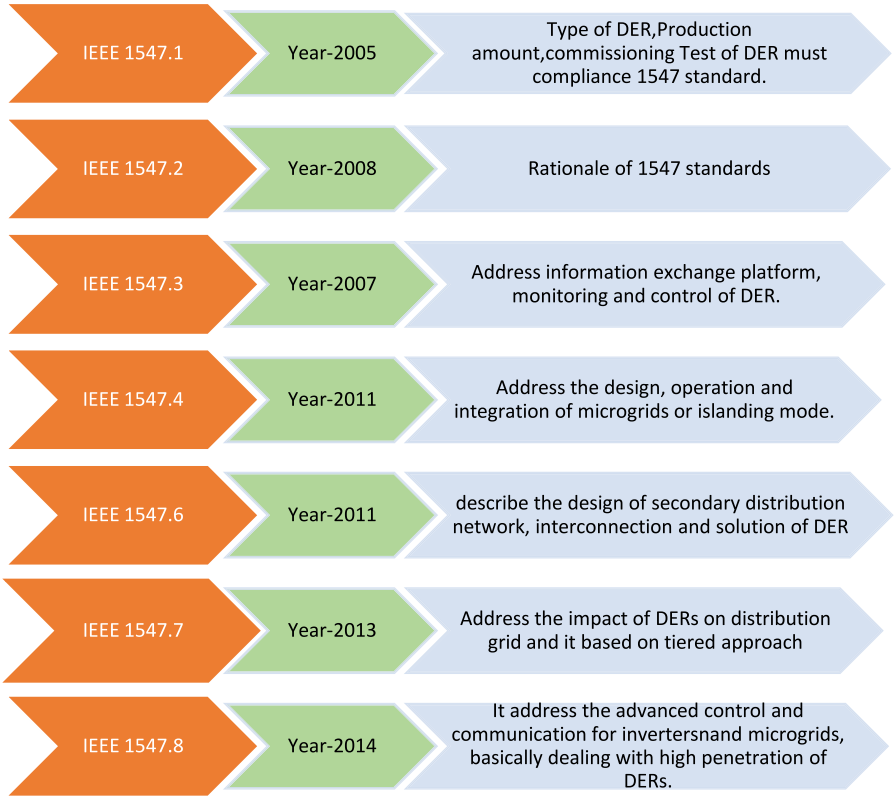

Fig. 3. IEEE standards for interconnection of DER.

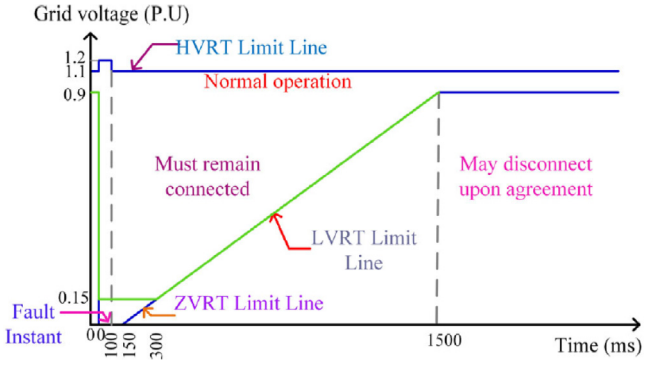

Fig. 4(a). FRT requirements as per German grid.

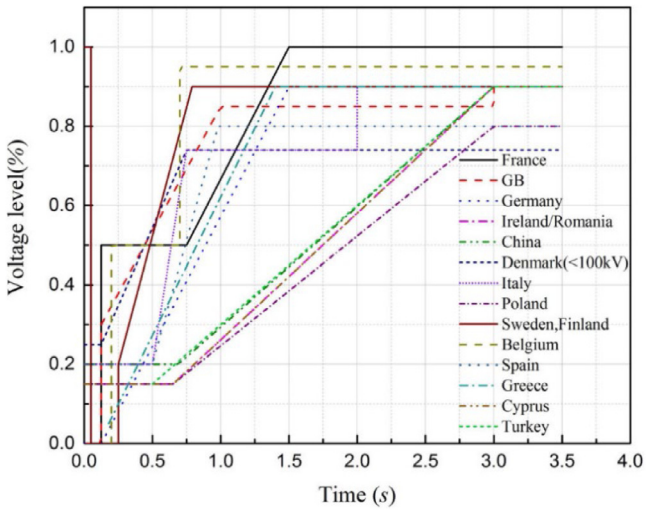

Fig. 4(b). Various countries FRT requirements.

renewable sources (Xue, 2017). Additionally, few tests are also incorporated for the integration of RES into grid. The FRT has the following test for wind plants, described in the international electrotechnical commission (IEC) 61400-21 document (Lamnatou et al., 2022):

i. Frequency control,
ii. Reactive power control
iii. Inertia control
iv. Test procedure for overvoltage and under-voltage ride through capability
v. Harmonic assessment

Moreover, many countries have framed their own grid code requirements, including the voltage operating range, frequency range, power factor range, fault duration, and restoration time. Table 3 lists the operating range defined by various countries during the occurrence of a fault (Ding et al., 2017; Gao et al., 2016; Xu et al., 2016).

2.2. Anti-islanding

In the anti-islanding mode, RESs detect abnormalities in the frequency and voltage and stop feeding electricity to the grid, which is mostly unintentional. Hence, it is concluded that the reliability and safety of grid operation depend on the frequency and voltage. Therefore, defining the variation limit for the frequency to avoid massive disconnections is important and challenging.

Table 3
Defined operating range as per grid code of different countries.

Country	Allowed operating voltages	Frequency Interval (Hz)	Fault duration (ms)	Fault restoration (s)	Power factor range	Grid code
France	EHV (400, 225 and 150 kV) and HV (90 and 63 kV)	47.0–52.0	140	1	0.85 lagging–0.92 leading	RTE
Germany	380, 220 and 110 kV 155 kV for offshore grid-connection	47.0–52.0	150	1.5	0.95 lagging–0.95 leading	E.ON
Great Britain	400, 275, 132 kV and below	47.0–52.0	140	1.2	0.95 lagging–0.95 leading	ESO
Ireland	400, 220 and 110 kV	47.0–52.0	250	0.75	0.95 lagging–0.95 leading	EirGrid
Romania	750, 400 and 220 kV	47.0–52.0	250	1.2	0.96 lagging–0.96 leading	ENTSO-E
China	EHV (1000, 750, 500 and 330 kV), HV2 (220, 110 and 66 kV)	48.0–51.0	140	0.7	0.97 lagging–0.97 leading	CEPRI
Denmark (<100 kV)	400, 220, 150 and 132 kV	47.5–51.0	140	0.75	0.95 lagging–0.95 leading	Energinet
Italy	380, 220 and 150 kV	47.5–51.5	500	0.8	0.95 lagging–0.95 leading	Terna
Poland	750, 400, 220 and 110 kV	47.0–52.0	150	3	0.95 lagging–0.95 leading	Polish
Sweden	400, 220 kV	47.0–52.0	250	0.75	0.95 lagging–0.95 leading	Swedish
Finland	400, 220, 110 kV	47.0–52.0	250	0.75	0.95 lagging–0.95 leading	Fingrid Oyj
Belgium	70–30 and 380–150 kV	47.0–52.0	200	0.7	0.925 lagging–0.90 leading	Elia
Spain	220, 132, 66 kV	47.0–52.0	500	1	0.95 lagging–0.95 leading	REE
Greece	150, 66 kV	47.0–51.5	170	1.5	0.85 lagging–0.90 leading	HTSO
Cyprus	132, 66, 22, and 11 kV	47.3–52	150	0.5	0.85 lagging–0.95 leading	CTSO
Turkey	380, 220, 154 and 66 kV	47.5–52.5	420	3	0.95 lagging–0.95 leading	TEIAS
India	400, 220, 132, 110, 66 and 33 kV	47.5–51.5	160	3	0.95 lagging–0.95 leading	IEGC

The standard, IEEE 1547, recently updated the grid code for islanding operation. In addition, IEEE P2030.8 in 2017, IEC 62898-1 in 2018 and IEC 62898-3 in 2020 released technical specifications for islanding operation (Rebollal et al., 2021). Moreover, in European Committee for Electrotechnical Standardization (2015), for detecting unintentional islanding, the intentional delay is provided, such as for frequency, a window from 47.5 to 50.5 Hz with a setting of 0.19 Hz/s using the ROCOF method. Table 4 consolidates the frequency limits provided for stable operation in few countries (Jawad and Massod, 2022; Eirgrid, 2015; ECM, 2017) and a typical active power–frequency curve is shown in Fig. 5.

Table 4
Limit for frequency for the normal operation in various countries.

Country	Limits of frequency (Hz)
Germany	$47.5 < f < 51.5$
Denmark	$48.5 < f < 51$
Spain	$47.5 < f < 51.5$
Canada	$59.4 < f < 60.6$
China	$49.5 < f < 50.2$
USAePREPA	$57.5 < f < 61.5$
USAeNERC	$58.5 < f < 61$
East of Japan	$47.5 < f < 51.5$
West of Japan	$58 < f < 61.8$
Australia	$47.5 < f < 52$
South Africa	$49 < f < 51$
Malaysia	$47 < f < 52$
Ireland	$49.5 < f < 50.5$
Romania	$47.5 < f < 52$
UK	$47.5 < f < 52.0$

2.3. Reactive current support

Reactive power injection or absorption plays a vital role in supporting the grid voltage stability. System operators also set rules for the reactive power flow during fault conditions. The active power output of the wind generator indicates the requirement for reactive power. As wind-generating units mainly contribute to the sharing of the grid load, it is important to derive a possible solution to support the grid voltage. As per regulations, wind units cannot disconnect at the time of the fault, but they have to take care of the voltage level by compensating for the reactive power and returning to normal operation after recovery. However, most grid codes consider 150 ms as the fault clearance time for the primary protection system and 250 ms in the case of a circuit breaker failure (Duong et al., 2018). The Danish grid code issued a regulation that grid-connected wind turbine generators deliver 1 p.u. active power along with reactive power to support the grid voltage (Gholizadeh et al., 2018). Fig. 6 shows the RES compliance of the German grid code for the reactive current support capability of the grid voltage (Xue, 2017). A ±10% dead band zone was provided to avoid unnecessary reactive power

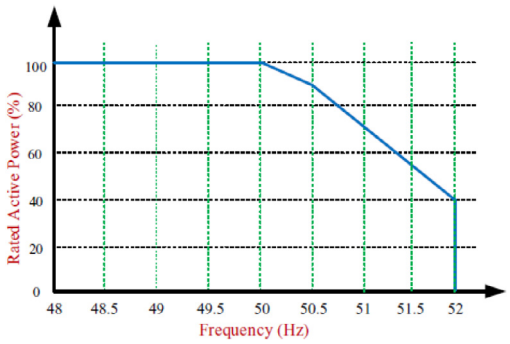

Fig. 5. Typical active power–frequency curve (Gkavanoudis and Demoulias, 2015).

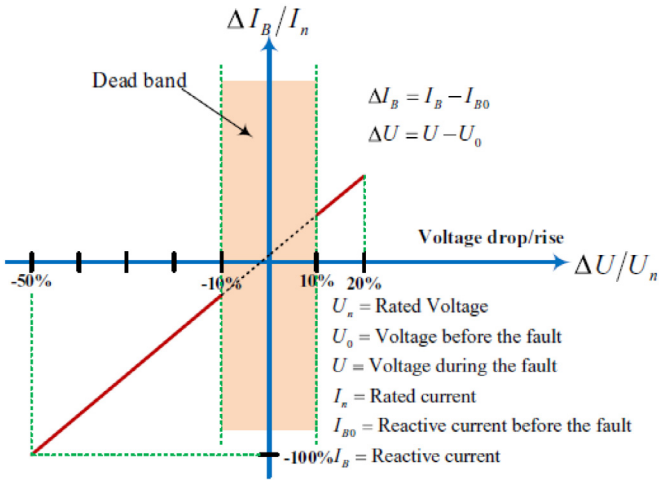

Fig. 6. A curve of reactive current to support the voltage at the time of fault (Etxegarai et al., 2015).

injection. Thus, the reactive current injection support to the grid is activated if the voltage dip is more than ±10%. This support were provided in conjunction with FRT types (Etxegarai et al., 2015).

i. LVRT during under voltage to inject the reactive power.
ii. ZVRT to increase the recovery time of the voltage.
iii. HVRT to absorb reactive power.

3. LVRT for generic RESs

Low-voltage ride through is a state in which all RESs must remain connected for a certain time to ensure that the fault is temporary. The LVRT operation for generic RESs is based either on the logic of various states, such as idle, freeze, connected, and disconnected, as shown in Fig. 8, or the curve defined by CEA, as shown in Fig. 7. A description of the states is given in Table 5 (Hil, 2020). The LVRT function is activated whenever an input voltage dip occurs.

All RESs unit are integrated with the grid at a point known as the point of common coupling (PCC). Whenever a fault occurs, a voltage dip occurs at the PCC. Therefore, in Fig. 9, the voltage profile of the PCC is observed with respect to time. In Area "A" RESs work normally. If voltage profile at connection point falls in Area "B", RESs remain connected for a certain time but in Area "C" RESs connection is allow to trip. The voltage level and time shown in Fig. 8, varies as per the country grid codes, as shown in Table 6 (Hassan et al., 2020; Cabrera-Tobar et al., 2016; Jerin et al., 2018). where,

V_n = Nominal Voltage (p.u.)
V_F = Voltage at the time of Fault (p.u.)
V_{AF} = Voltage after Fault (p.u.)
T_F = time at which voltage drops due to Fault (s)
T_r = Recovery time (s)

In addition, disturbances in the generating system leads to a voltage dip known as a brownout condition. In the brownout condition, RES must be connected to the grid and support the grid by providing reactive power to raise the system voltage. A connection during the voltage dip is necessary owing to the high share of RESs in the distribution grid.

3.1. LVRT requirement in wind power plant

According to the global wind report-2021, the total new onshore and offshore installed wind power capacity is 93 GW, as shown in Fig. 9. In addition, detailed installation reports of wind power plants in each country are clearly described in the report (Feng et al., 2021). Fig. 10 shows the worldwide percentage share of new onshore and offshore wind power, which will increase multiple times in the near future. In contrast, large wind power plant significantly affects the steady-state and dynamic operation of the electrical power system. However, operators have specified the standard operating codes for both operating states to ensure smooth operation. During steady state, the plant must follow the frequency and voltage limits (Sourkounis and Tourou, 2013). The various wind turbine generators unit with their LVRT block diagram are described in the further section.

The LVRT implementation for wind plants depends on the type of generator being used. Therefore, it is essential to consider the various types of generators used in wind plants, as shown in Fig. 10 (Karaağaç, 2020). A systematic review of various wind generators types is provided by Devashish (Jha, 2017).

The squirrel-cage induction generator (SCIG) operates either at a fixed speed or at two-speed modes. Riding through the low voltage by SCIG during a fault is explained in Gholizadeh et al. (2018). A block diagram of the LVRT capability of the SCIG is shown in Fig. 11 (Gholizadeh et al., 2018). It is evident from Fig. 11 that many auxiliary and peripheral devices are required to bypass tripping at low voltages. These auxiliary devices are further divided into three categories: series, shunt, and hybrid, as explained by Gholizadeh et al. (2018).

In contrast, two types of synchronous generators, wound rotor synchronous generators (WRSG) and permanent magnet synchronous generators (PMSG) are being used for wind plants. However, author Jian et al. (2022) proposed a LVRT control strategy for a wind turbine with PMSG based on operating simultaneously of rotor energy storage and a discharging resistance. These generators are directly driven with a maximum power rating of 7.5 MW (Karaağaç, 2020). The LVRT capability handling block for the PMSG with controllers is shown in Fig. 12 (Erlich et al., 2017). Controllers types with their connections and limitations are systematically summarized in Kasem et al. (2018) and Gholizadeh et al. (2018).

Whereas, a doubly fed Induction Generator (DFIG) is the most effective type of generator. Wind turbines are mostly implemented using DFIG, as the converter power rating is 30% of the rated power of the machine (Redlinger et al., 2016). In the DFIG, the stator is directly coupled with the grid, whereas the rotor is connected to the grid via power converters. This enables generator-side active and grid-side reactive power control. In Tan et al. (2020), the authors presented a cut-out strategy that works

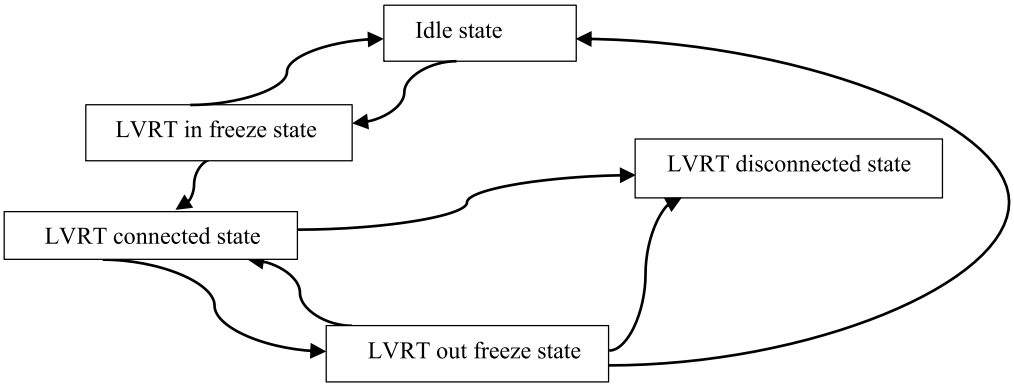

Fig. 7. Various LVRT states (Hil, 2020).

Table 5
LVRT states description (Hil, 2020).

State-No.	State name	Function
1	Idle	If $V_{PCC} \leq V_{PCC(previous)}$, state 2 will become active.
2	LVRT in freeze	After $\frac{1}{f_{DERs\ nominal}}$ seconds, PCC voltage has recorded. LVRT logic return to 1, if this voltage is greater than previous recorded voltage at PCC, otherwise go to the next.
3	LVRT connected	1. During this stage, all the DERs remains connected. 2. Active and reactive power contributions applied. In addition, connection timer is continuously update. 3. If $t_{internal} \geq t_{calculated}$, LVRT logic goes to state 5 means disconnection. 4. Either $V_{DERs} \geq V_{Previous}$ or $V_{DERs} \leq V_{first}$, LVRT logic goes to state 4.
4	LVRT out freeze	After $\frac{1}{f_{DERs\ nominal}}$ seconds, DERs voltage is recorded and LVRT logic varies as per below mentioned point. 1. $V_{DERs} \geq V_{Previous}$, LVRT logic goes to state 1. 2. $V_{DERs} \leq V_{first}$, LVRT logic goes to state 5 if possible otherwise state 3.
5	LVRT disconnected	Stay in this state until the voltage at PCC recovered.

Table 6
International grid standards during LVRT.

International grid standards	At the time of fault		After the fault	
Country	V_F in per unit	T_F in seconds	V_{AF} in per unit	T_r in seconds
Ireland	0.15	0.625	0.90	3
Germany	0	0.15	0.90	1.5
India	0.15	0.3	0.85	3
China	0	0.15	0.90	2
Denmark	0.25	0.15	0.75	0.75
Italy	0.20	0.50	0.90	2
Spain	0.20	0.50	0.95	1.50
Canada	0.15	0.625	0.90	3
USA, Puerto Rico	0.15	0.60	0.85	3
South Africa	0	0.15	0.85	2

with LVRT capability. In Kasem et al. (2018), the authors proposed a modified strategy in which the crowbar resistance was used to limit the rotor current. In Hiremath and Moger (2022), author proposed algorithm-Modified Super Twisting algorithm based sliding mode control for the enhancement of LVRT for DFIG wind plant. A systematic review on LVRT in wind energy conversion system and fixed speed wind power generator system is presented in Howlader and Senjyu (2016) and Moghadasi et al. (2016). In addition, this strategy forces the wind plant to operate during transient faults. The LVRT capabilities handling blocks for the DFIG with controllers are shown in Fig. 13 (Erlich et al., 2017).

In addition, induction-type wind turbines are used because they can absorb reactive power during start up and normal operation. Owing to the variable output characteristics of wind power plants, multiple starting times in a day lead to fluctuations in the absorption of reactive power and require reactive power compensators, such as switched capacitor banks (Mali et al., 2014). Several measures have been taken to mitigate the effects of reactive power generation. Static var compensators or STATCOM are dynamic reactive power compensators with LVRT capability provided at the RE pooling station to support the grid in undesirable conditions of reactive power flow (Amalorpavaraj et al., 2020).

Therefore, it can be concluded that LVRT must be define at the time of planning based on the wind turbine for ride through during fault. Various countries have their different LVRT requirement such as in North America wind plant remain connected till voltage level goes down 15% of the rated voltage with the time period of 625 ms (Hossain et al., 2012), German plant work continuously with 0% voltage dip with 150 ms time duration to resume the power after that plant should be disconnected (Abulanwar, 2016). Technical issues due to the penetration of wind

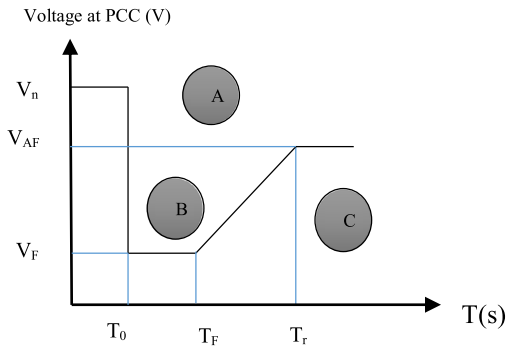

Fig. 8. Basic diagram of LVRT.

energy into the grid, the Indian wind energy grid code (IWGC), introduced requirements related to the connection code, power balance, reactive power support, fault ride through capability, protection, and the ability to withstand the wind plant during faulty conditions. In 2013, the Central Electricity Authority (CEA) issued the LVRT requirement for a wind power plant integrated into the main grid at 66 kV and above. Below 66 kV, the fault ride through requirement is not required (Muyeen et al., 2009). The wind power plant must be connected to the grid at the time of the system fault and supply active power proportional to the voltage drop. In addition, the grid is supported by injecting a reactive current with the specified time given in the grid code. Generally, for a low-voltage grid, the wind power plant (WPP) is connected to the grid with a time duration of 140 ms, whereas it remains connected for more than three minutes (Tsili and Papathanassiou, 2009).

The small wind power plant should be capable of withstanding repetitive faults, as fault occurrence on sub-transmission is frequent and specific measures have already been taken. The small plant should operate within the frequency range of 47.5 to 51.5 Hz and maintain the power factor within the specified limit. The BIS (Bureau of Indian Standards) restricts the upper limit of the frequency–wind turbine sectional committee ET 42 (Hansen et al., 2021).

The IEC (International Electrotechnical Commission), an organization, published a standard for power quality known as electromagnetic compatibility (Ward, 2001). Fig. 14 compiles the four possible solutions for LVRT capability, which can be considered for WPP.

3.2. LVRT requirement in solar power plant

The market for solar PV declined the cost of the panel by approximately 63% over a span of 8 years (Fu et al., 2018). Moreover, the share of grid-connected solar PV crossed the grid-connected wind plant share. In Jawad and Massod (2022), the fault ride through enhancement approaches for the solar plant were classified into two groups based on the controller type and connection type. These groups are exposed to controller-based and external device-based approaches. Furthermore, the controlled-based approach includes a modified inverter controller and computational approaches, whereas the external device-based approach includes energy storage, FACTS devices, braking choppers, and fault current limiters. Finally, the author concludes that energy storage and FACTS devices in the external-based approach and the modified inverter controller in the controller-based approach are the best, as the modified inverter controller has the capability to retain the inverter connection and can inject the required power to support the grid voltage during the fault.

Hassan et al. (2020) examined and described various current injection techniques for grid-connected PV with LVRT control strategies and controller capability. Fig. 16 shows the various current-injection techniques with control strategies under LVRT requirements. Controllers are implemented to regulate the active and reactive power injection during LVRT. The author also provided detailed description of the differences in strategies. However, author Mojtaba Nasiri et al. deployed a braking chopper with a controller that follow the grid code for controlling the LVRT but for single stage grid integrated solar PV system (Nasiri et al., 2022). The current compensation control has voltage/current sequence control capability, reactive current injection (RCI) has constant, variable and maximum current control capability, linear method has frame control, and non-linear method has frame control capability. Kheng Heong Oon analysed the five various RCI control (Oon et al., 2018). The author of Parvez et al. (2016), has proposed a current control method based on linear and non-linear current control. These categories are shown in Fig. 15. Moreover, the author concluded that the proportional resonant (PR) controller seems best to ride through during fault conditions, as it can compensate harmonics and has high dynamic performance.

However, the sudden increase in the output current of a solar plant causes LVRT failure; therefore, the authors of Zhou et al. (2008) showed an effective technique to suppress the sudden surge in output current, using the voltage feed-forward approach in the control loop of dynamic voltage restorer. The grid-tied PV has inverters, such as a voltage source inverter, to convert the captured DC energy into AC. These inverters are prone to disturbance, and unsymmetrical faults create a lot of disruption due to the presence of negative sequence components, leading to DC link voltage fluctuations (H et al., 2014). A test setup for PV inverters for research on HVRT and LVRT is created (Li et al., 2021).

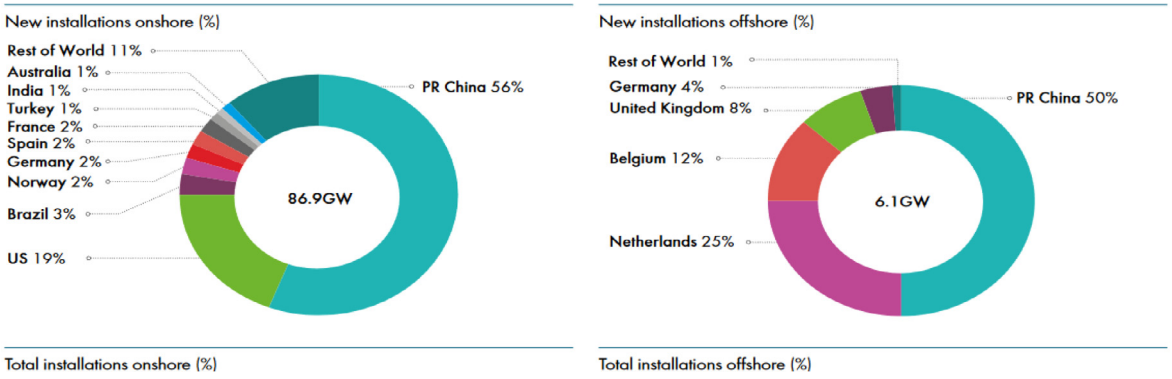

Fig. 9. Share of new wind power onshore and offshore.

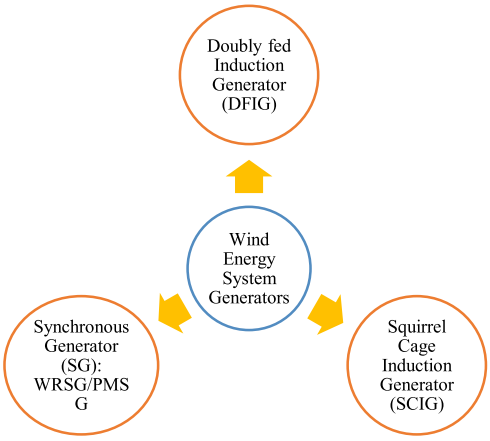

Fig. 10. Wind energy system generators.

Earlier LVRT requirements were considered only for wind turbines, as a three-phase fault on a transmission line makes zero voltage at the point of fault until the clearance of the fault leads to power loss. Currently, there is a boom in the development of integrated solar power plants. During disturbances or faults, the shutdown of complete power generation from the solar power plant is unreliable, resulting in blackout conditions. Hence, it is proposed that an LVRT certification test is required before RE is integrated into the grid. LVRT tests for photovoltaic systems are normally performed in the laboratory using LVRT test setups.

4. Control strategies for FRT

Various LVRT techniques have been proposed in the literature for grid support. A block diagram of a solar power plant connected to a grid is shown in Fig. 16, which includes a converter, DC link capacitor, control algorithm, grid interface inverter, and a star-delta connected transformer. The output of the inverter includes high-order current and voltage harmonics, and to reduce these harmonics, an inductive filter is connected. However, voltage appears on the DC link connected to the PV array, which is the main concern for LVRT. The author in Muaelou et al. (2016) proposed a control strategy that generates reactive power under faulty conditions and is capable of FRT.

According to the author in Nivedh et al. (2017), if a fault occurs and the voltage drop is 20% of the rated voltage for an approximate time of 550 ms, then the solar plant must inject a reactive current of approximately 100% of the rated voltage to support the grid. After fault clearance, the active power output will increase within 160 ms. In addition, the author reviewed various field tests, measurements, and evaluations, and proposed a testing procedure in line with the CEA requirements for the wind turbine (WT) and solar.

Yuan et al. (2013), concluded that during LVRT, when an overvoltage appears at the DC link, it can control the input power. The variation in the firing angle led to a maximum power-point deviation. Yin and Xu (2014) suggested that excess input power could be controlled by shunting a suitable value of the resistor across a DC link through a switch. Moreover, the input voltage is first compared with the reference voltage and then applied to the DC-link capacitor. If the voltage is greater than the reference voltage, the excess voltage is discharged through the resistor. Results of the above study shows a decrease in solar power efficiency for a small duration while controlling the input power given to the DC link capacitor. To mitigate this effect, an energy storage and circuit breaker control strategy was developed by Manikanta et al. (2017). In this technique, the maximum power point controller compares the DC link voltage with the nominal voltage. If the voltage is within the specified limit, the boost converter remains in the OFF condition; otherwise, the controller sends a signal to the converter, which lowers the extra voltage by charging the battery.

The literature on LVRT grid code in PV-connected systems revealed that an efficient DC link voltage control method is required. The author in Joshi et al. (2021) and Li et al. (2022), systematically described various current, voltage, and reactive power support strategies during low-voltage ride through. Figs. 17 and 18 show the list of control strategies used to support the voltage, DC-link voltage, and reactive power.

5. Simulation for LVRT test capability

To test the LVRT capability, initially steady state load flow analysis was performed to determine the operating state of the network on the DIgSILENT software. The limits of active and reactive power should be defined initially, as shown in Fig. 19, and can be changed at any time as per the requirement. In addition, the minimum and maximum limits of the reactive powers of the static generator are defined by the capability curve, as shown in Fig. 19 (DIgSILENT, 2022). The capability curve defines the boundaries for the reactive power flow without overheating. The P_{max}, P_{min} limits of active power are shown horizontally in the capability curve, whereas the Q_{max}, Q_{min} limits of reactive power are shown vertically. In addition, the thick blue semicircle in the curve shows the operational or power limit of the generator; within this area, the generator can work effectively without much system loss.

5.1. Scenarios to test LVRT capability in wind farm

A wind farm with six WT models was connected to an external grid of 20 kV at the point of common coupling (PCC) to support the demand, as shown in Fig. 20 (Joshi et al., 2021).

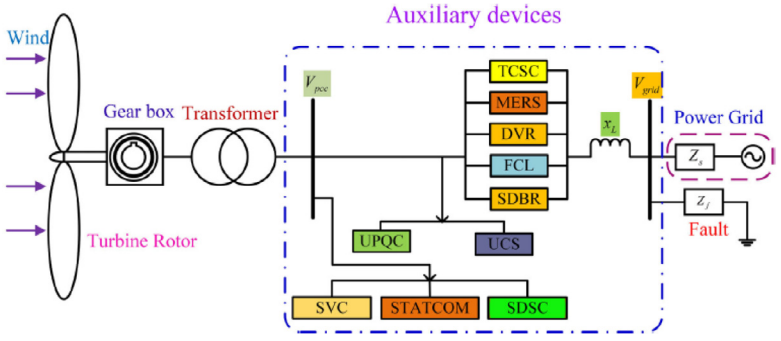

Fig. 11. Block diagram representing the LVRT capability of squirrel cage induction generator (Gholizadeh et al., 2018).

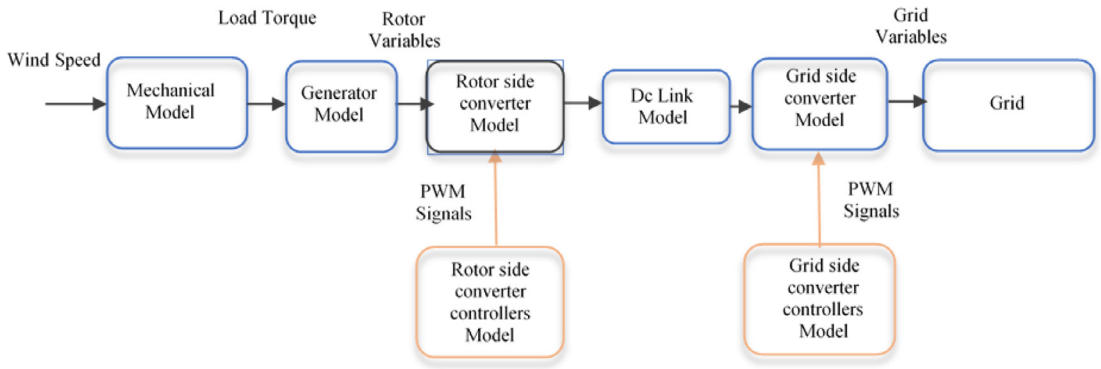

Fig. 12. Block diagram representing the LVRT capability in PMSG with controllers.

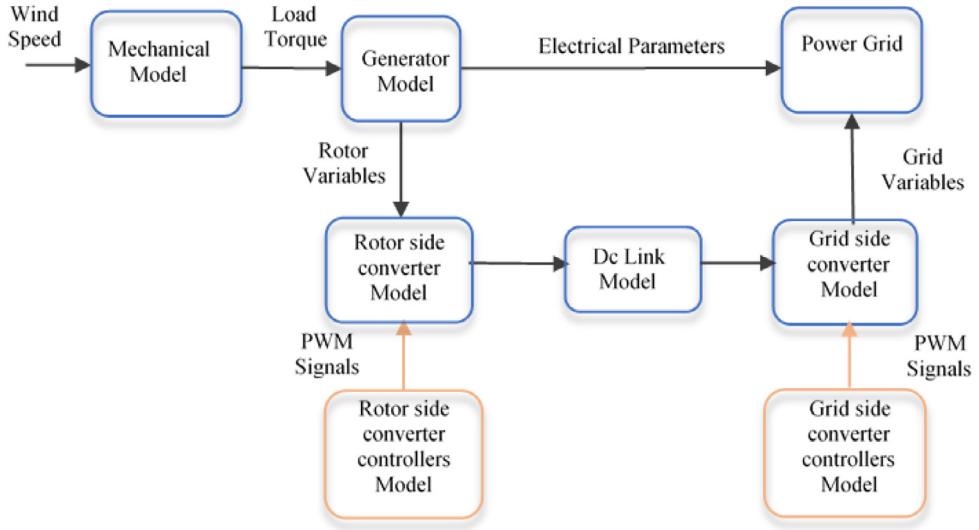

Fig. 13. Block diagram representing the LVRT capability in DFIG with controllers.

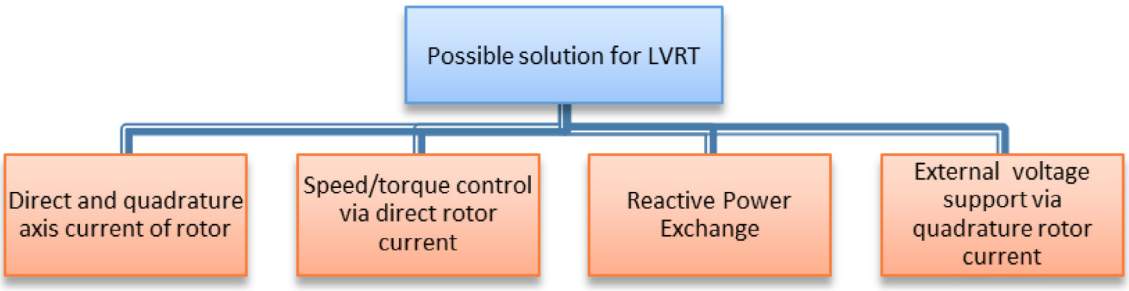

Fig. 14. Possible fault ride through techniques.

Each wind turbine model includes a sub-model of its control system, which includes a PQ controller, voltage and current measurement devices, and PQ measurement devices. A systematic block diagram of the composite model frame containing the measurement devices and controllers with their connections is shown in Fig. 21. The associated values of PQ controller are provided in Table 7.

To test the LVRT capability, a fault is applied near the point of common coupling (PCC), and two cases have been considered. (i) fault without fault impedance and (ii) fault with inclusion of fault impedance.

5.1.1. Scenario I: Fault applied near to PCC without fault impedance

To understand the behaviour of the LVRT in the wind farm, a fault is created very close to the PCC, which causes the voltage at that point to fall to zero. The turbines in the wind farm are configured to inject additional reactive current into the network to support the voltage in the event of a fault (Fig. 20). A dynamic simulation has been performed on the DIgSILENT PowerFactory software for stability analysis in transient period. Thenceforth, a three-phase short-circuit fault is applied at zero seconds and cleared after 500 ms. The short-circuit fault was simulated at bay-3, and the location of the fault is shown in Fig. 22. As no fault impedance is considered, the voltage at the bus drops to zero.

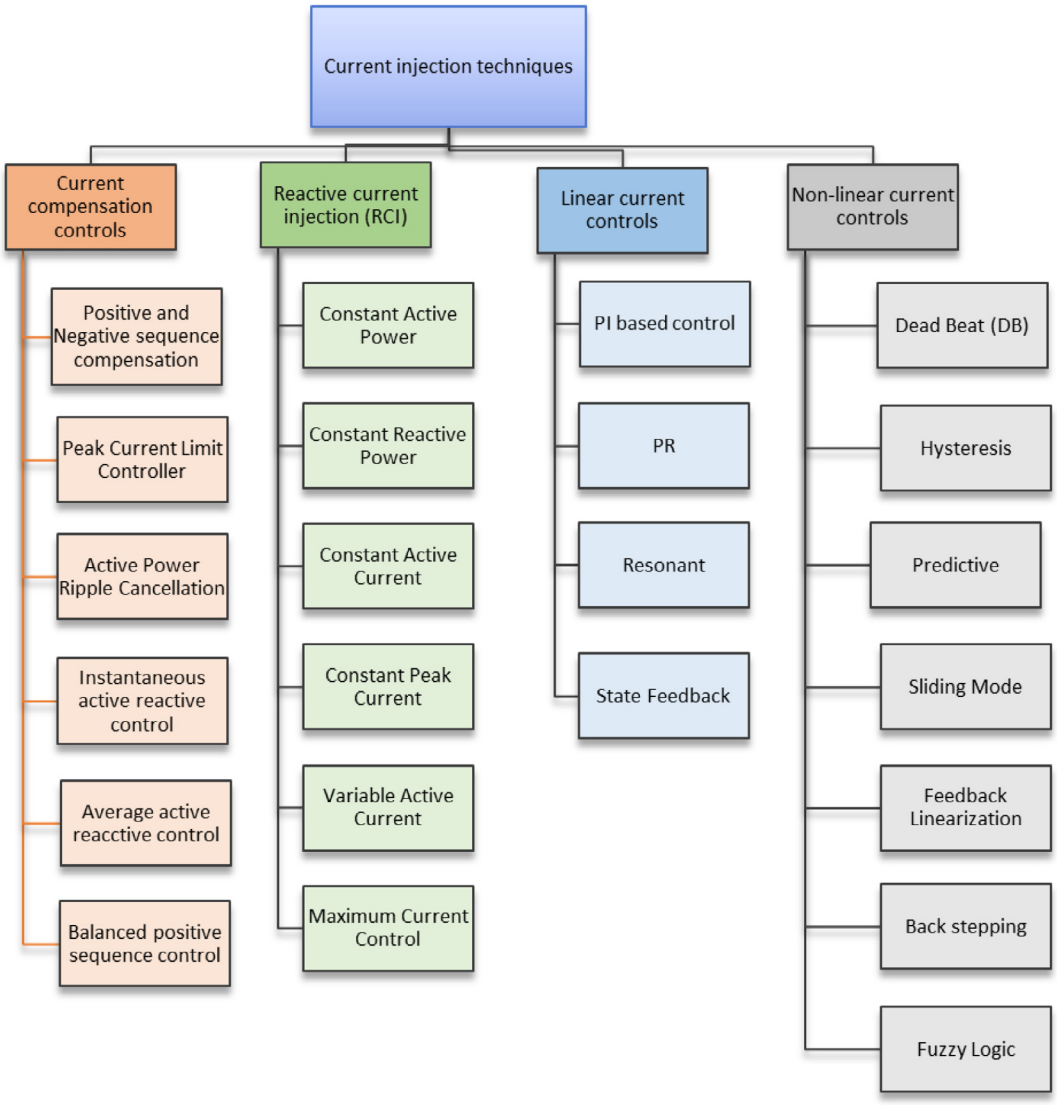

Fig. 15. Various current injection technique for grid connected PV used under LVRT requirement (Hassan et al., 2020).

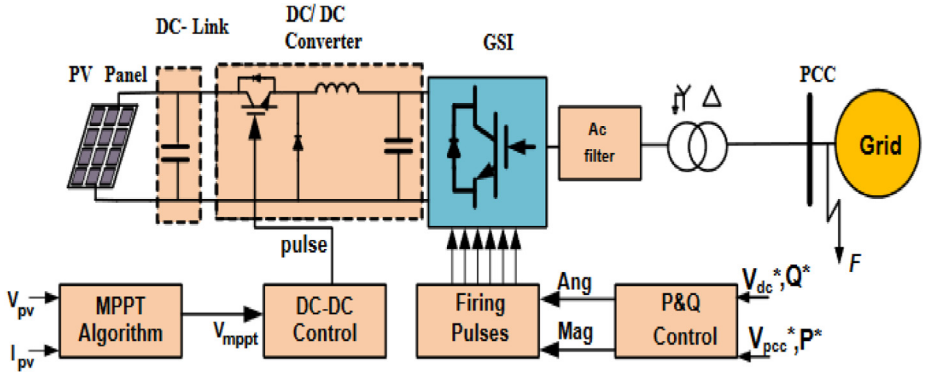

Fig. 16. Block diagram of integrated solar power plant to grid (Zhou et al., 2008).

The relation between the fault impedance (Z_f) and the nominal voltage (V_n) is given in Eq. (1):

$$Z_f = \frac{V_n}{I_f} \tag{1}$$

Or,

$$V_n = Z_f * I_f \tag{2}$$

Therefore, when, $Z_f = 0$, V_n becomes zero from Eq. (2).

Table 7
PQ controller parameters value.

Parameters	Symbol	Values (Per unit)
Active power control gain	K_p	0.5
Active power control time constant	T_p	0.04
Reactive power control gain	K_q	0.5
Reactive power control time constant	T_q	0.01
Voltage dead band	deltaU	0.1
Filter time constant rms voltage	Tumeas	0.007
Reactive support gain	K_ deltaU	2
Combined current limit	i_ max	1
Max. allowed internal voltage	u_max	1.1
Coupling reactance in %	X	10
Max. gradient at normal voltage (%/s)	dP_{max}	200
i_d current limit	i_{d_max}	1
i_q current limit	i_{q_max}	1
Max. limit of active reference power	P_{ref_max}	1
Max. limit of reactive reference power	Q_{ref_max}	0.4
Gain of active current controller	K_d	1
Integrator time constant	T_p	0.002

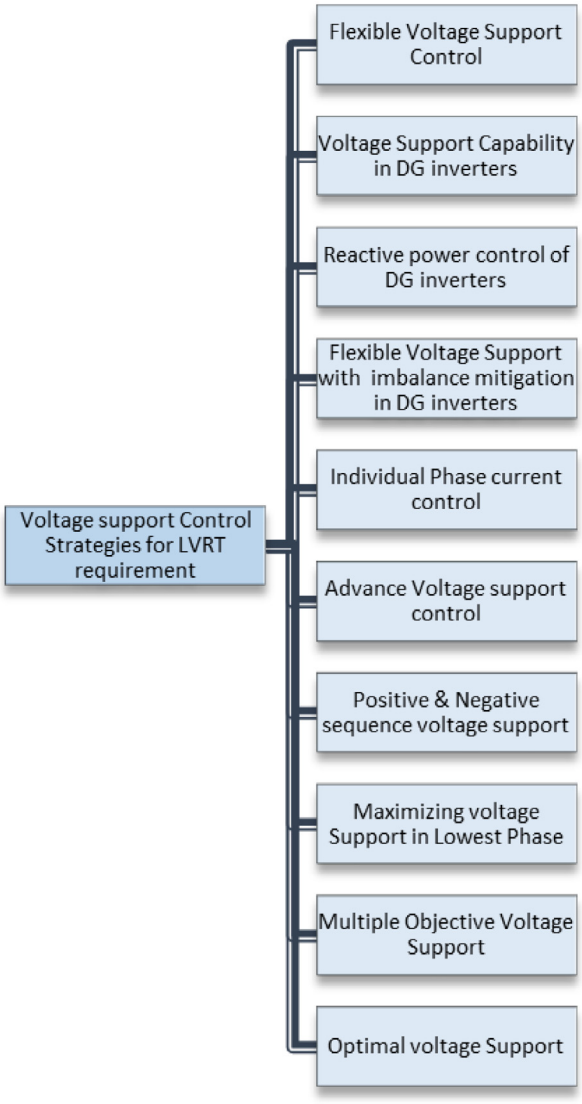

Fig. 17. Various voltage support control strategies for LVRT requirement.

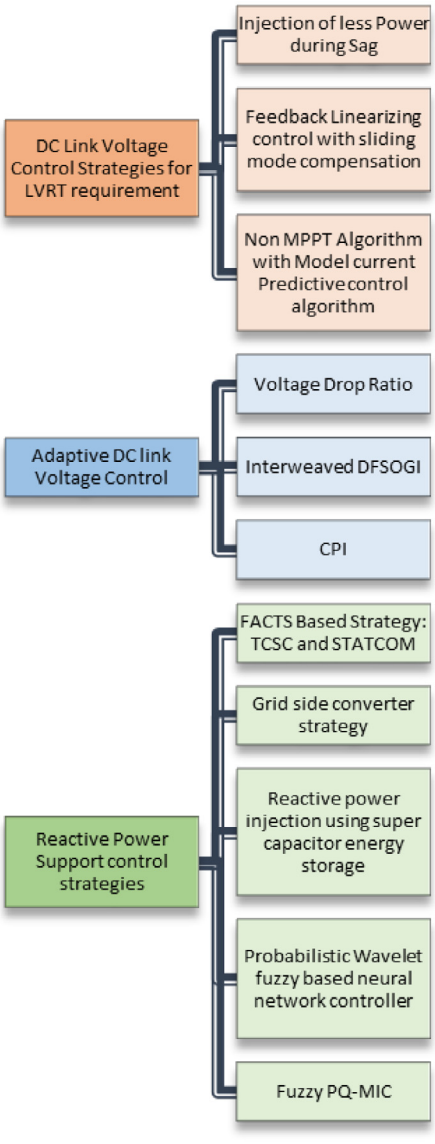

Fig. 18. Various DC link voltage and reactive power support control strategies for LVRT requirement.

After 500 ms, the highlighted circuit breaker switch opens to clear the fault, as shown in Fig. 22.

To calculate the initial condition, a balanced RMS simulation (dynamic) was carried out for absolute 1 s The output waveform

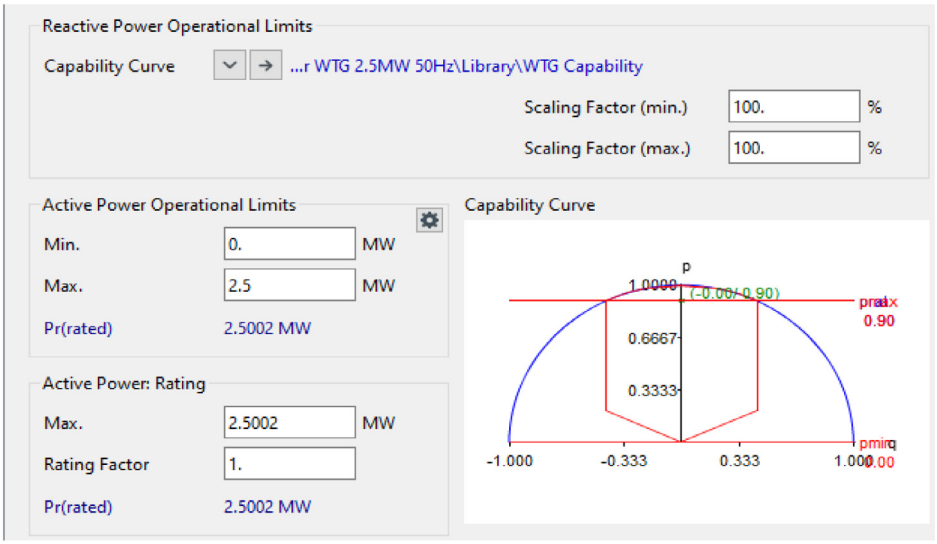

Fig. 19. Capability curve for wind generator. (For interpretation of the references to colour in this figure legend, the reader is referred to the web version of this article.)

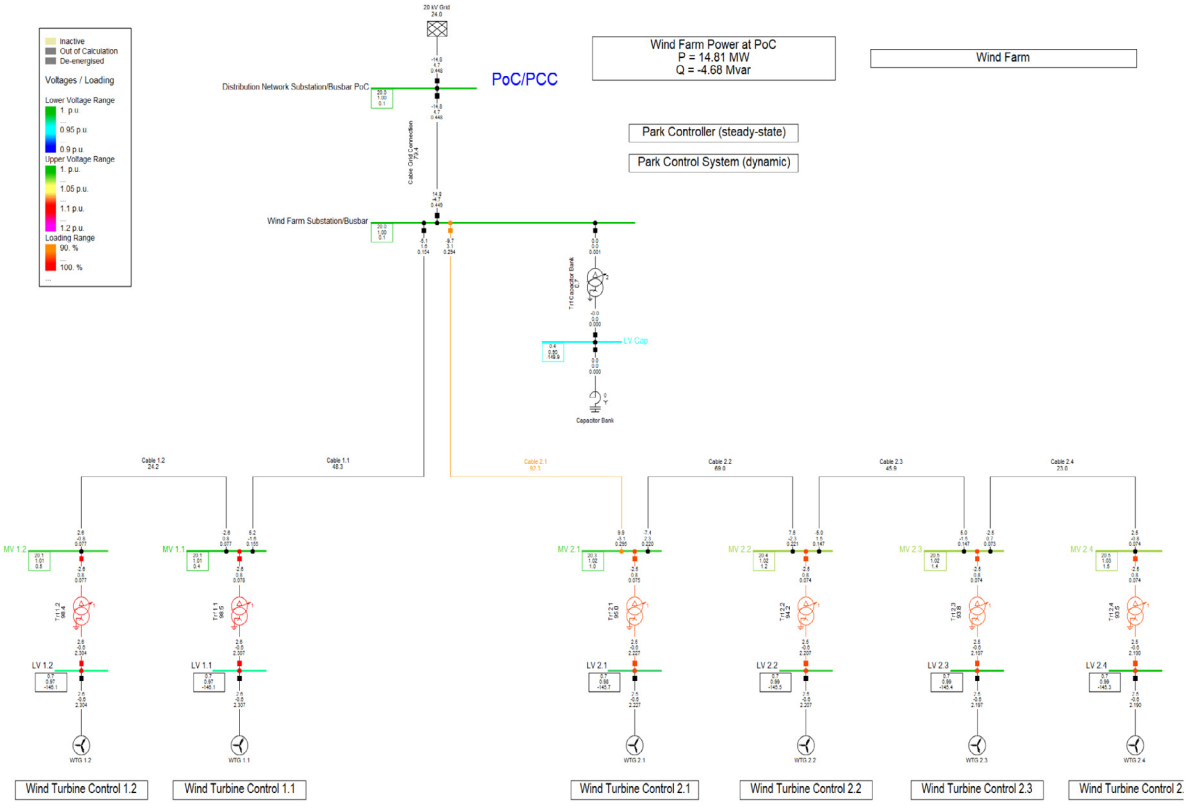

Fig. 20. Wind farm connected to grid.

of the simulation shows the variation in various parameters with respect to time, as shown in Fig. 23. Plot-1 shows the voltage at the bus bar of the wind farm substation. It can be seen that when the short circuit is applied at zero second, the voltage at the bus bar decreases to zero and remains at zero until the fault is cleared at 500 ms (highlighted in the figure). After 500 ms, the voltage returned to its pre-fault value. However, plot-2 shows positive sequence current contributions from the external grid and the wind farm. It is clear that the contribution from the grid during the fault is very high. Active and reactive power contributions from the wind farm are shown in plot-3, in which green and red indicate active and reactive power contributions, respectively. In addition, it can be seen that during the fault, because the voltage at the PCC drops to zero, the real and reactive powers also drop to zero.

The results associated specifically with one turbine (WT-2.4) are shown in Fig. 24. The first graph shows the positive-sequence voltage at the wind turbine terminals. It is evident that the voltage falls during the fault but does not collapse at the PCC because of the impedance between that point and the turbine. The bottom graph shows the active and reactive powers. It is observed that prior to the fault, the active and reactive current

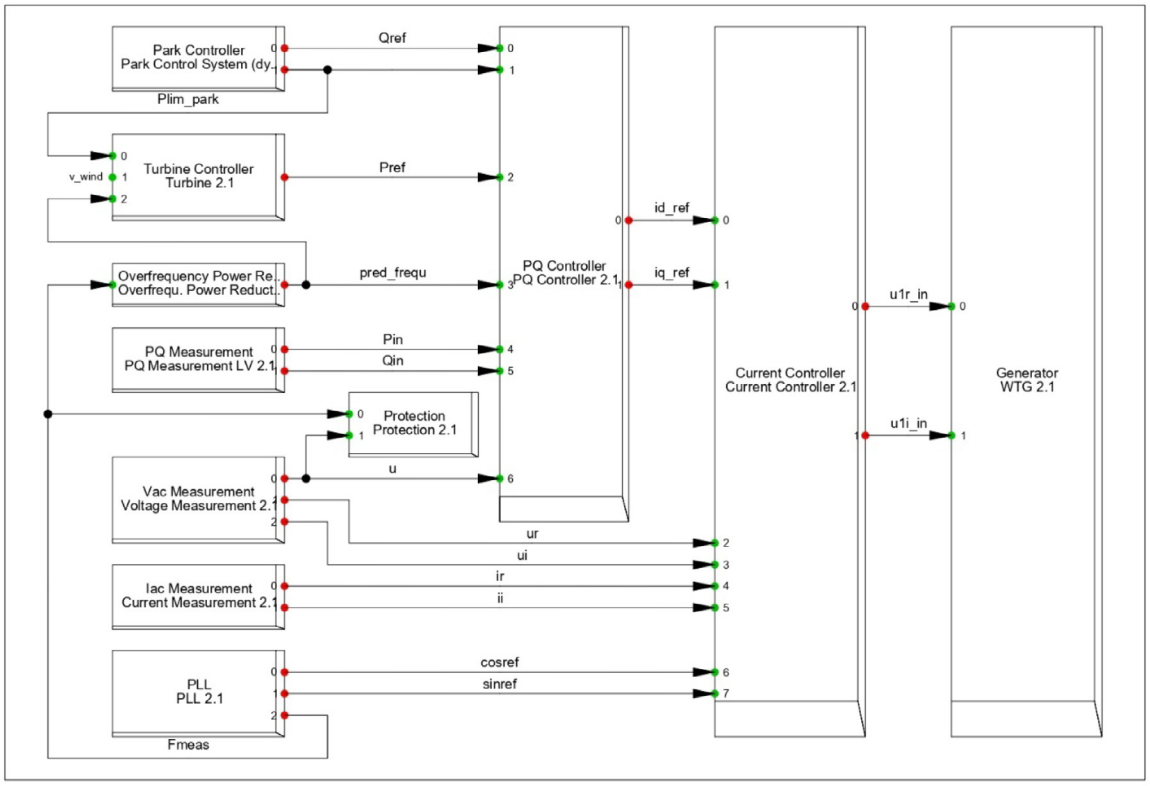

Fig. 21. Composite model frame of wind turbine containing measurement devices and controllers.

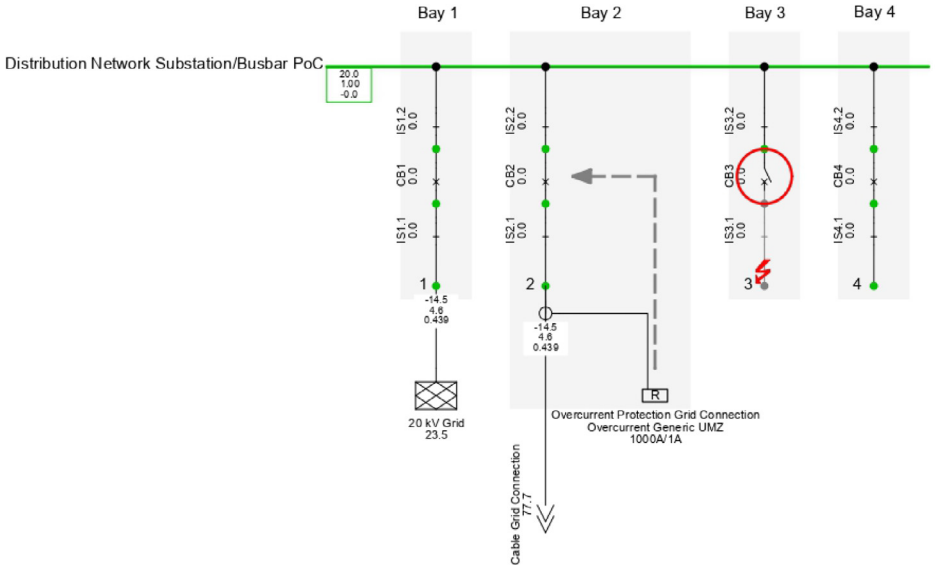

Fig. 22. Location of the short circuit fault.

are constant. As the fault is applied, there is an initial reaction from the wind turbine, and the voltage support mode for the full ride through begins to exert its influence. The reactive current delivered is determined by the voltage dip and k-factor. The k-factor is a gain for the additional reactive current required for voltage support, which is taken as 2 in this simulation and can be adjusted according to the requirement. However, the reactive current is increased, but the active current is reduced because priority is given to the reactive current injection. Moreover, the post-fault values returned to their pre-fault values.

5.1.2. Scenario II: Fault applied near to PCC with fault impedance

In Scenario II, a fault is applied near the PCC, but a fault impedance is included, which results in a voltage drop at the PCC to 30% of its nominal value. The simulation was carried out in a manner similar to scenario I. The fault clearance time was taken as 500 ms. Variations in the parameters after the execution of the simulation are shown in Fig. 25. Plot-1 shows the voltage at the bus bar of the wind farm substation, and the fault was cleared after 500 ms (highlighted in the plot). In this scenario, the voltage is not equal to zero, owing to the inclusion of the fault impedance, and the reactive power is higher than the active power.

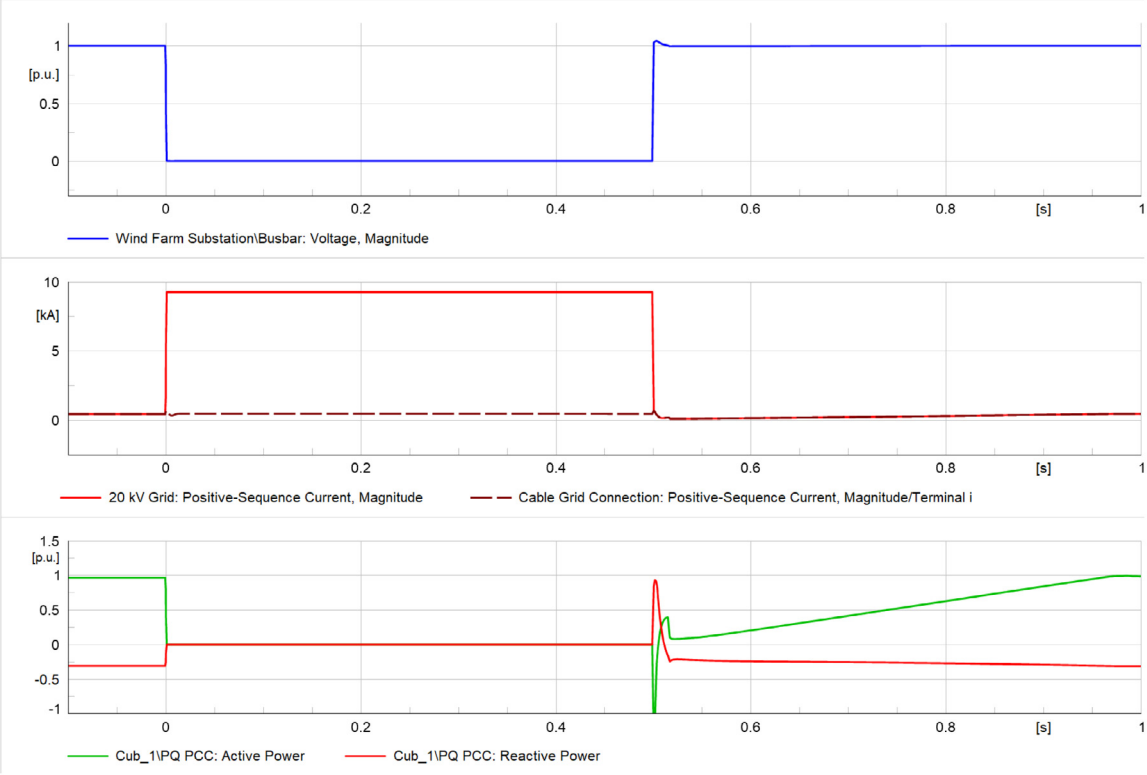

Fig. 23. Output waveform without fault impedance inclusion. (For interpretation of the references to colour in this figure legend, the reader is referred to the web version of this article.)

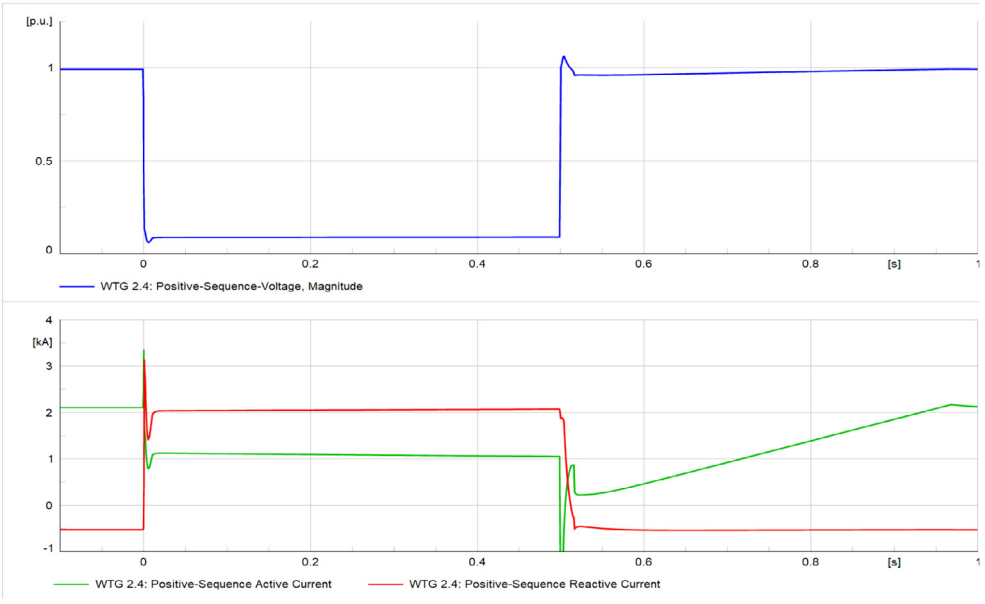

Fig. 24. Output associated with one turbine.

5.2. Scenarios to test LVRT capability in solar PV farm

To test the LVRT capability of the solar PV farm, a grid-connected solar PV farm was considered. For the load flow analysis of the system, the active and reactive values were initially given. The Fig. 26(a) shows the power values, which can be changed according to requirements. Fig. 26(b) shows the capability curve of the solar PV system. The reactive power is on the x-axis, and active on the y-axis. The thick blue semicircle shows the operational or power limit of the inverter; within this area only the inverter can work.

5.2.1. Dynamic simulation to examine the LVRT for solar farm

A generic model for low-voltage ride through is available in the PowerFactory software. This subsection presents the complete simulation of solar farm including various control block as shown in Fig. 27. The functions of each block are listed in Table 8. In previous section simulation of wind farm have been presented

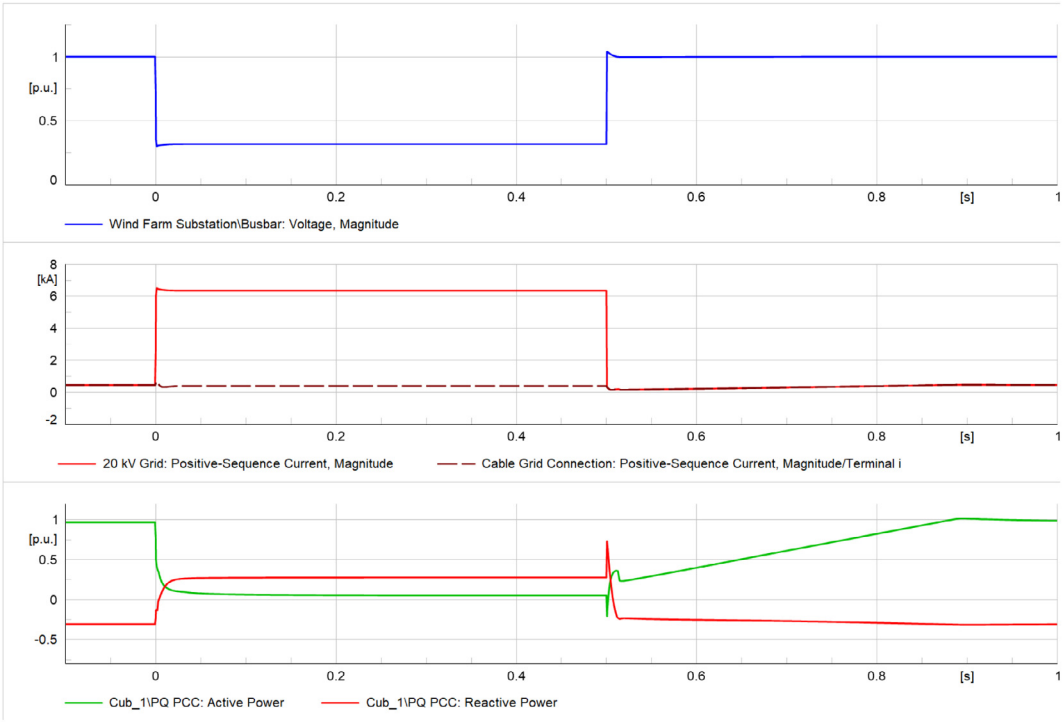

Fig. 25. Output waveform with fault impedance inclusion.

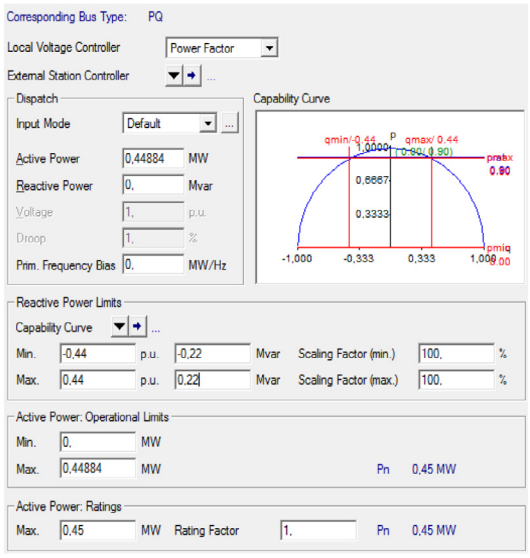

Fig. 26(a). PV power flow under steady state (Manikanta et al., 2017). (For interpretation of the references to colour in this figure legend, the reader is referred to the web version of this article.)

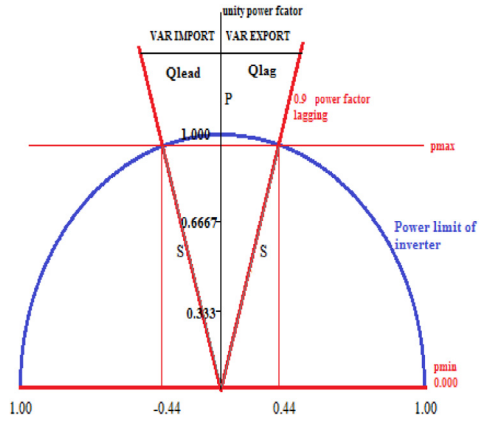

Fig. 26(b). PV capability curve. (For interpretation of the references to colour in this figure legend, the reader is referred to the web version of this article.)

including load flow as wind power plant has the rotatory machine and for the implementation of LVRT, inertia and rotation control are required. However, for the solar plants the controller requirement has been focused primarily as solar PV plant considered as a static generator, therefore, controlling the DC link becomes imperative for LVRT implementation.

5.2.2. Solar farm controller model

Static generators were integrated into the grid to test the low-voltage ride through capability. The input of the static generators comes from the controller, as shown in the generalized model, and the outputs are power. Moreover, the controller plays a key role in the regulation of static generator outputs, that is, active and reactive powers. A block diagram of the controller is shown in Fig. 28 (Mahmood, 2012). The entire controller system is segregated into three sub-blocks, represented by 1, 2, and 3. Block 1 maintains the active power flow, and block 2 is a reactive power support model, which is modelled based on German guidelines and used to regulate the reactive power during the voltage dip in the grid voltage. The final block 3 is a current limiter that provides the reference output values i_{d_ref} *and* i_{q_ref} and has a 10% deadband that can be change anytime as needed. Furthermore, if the voltage deviation is within ±10% of the nominal value, no injection or absorption of reactive power can occur (Mahmood, 2012), whereas if the voltage deviation is more than ±10% of the nominal value, reactive power support is provided to the grid to improve the voltage profile.

The operation of LVRT driven controllers for two different scenarios e.g. normal transient faults and transformation into

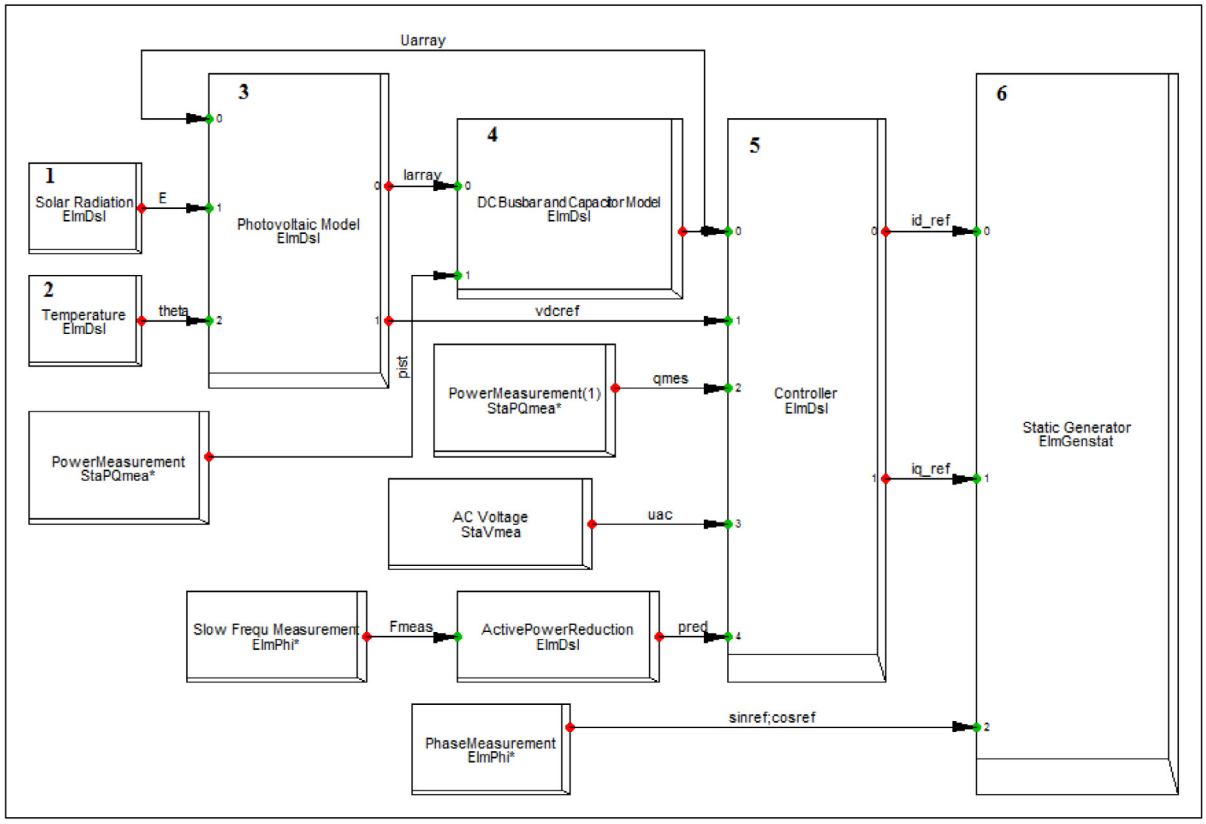

Fig. 27. Composite model frame of PV containing measurement devices and controllers.

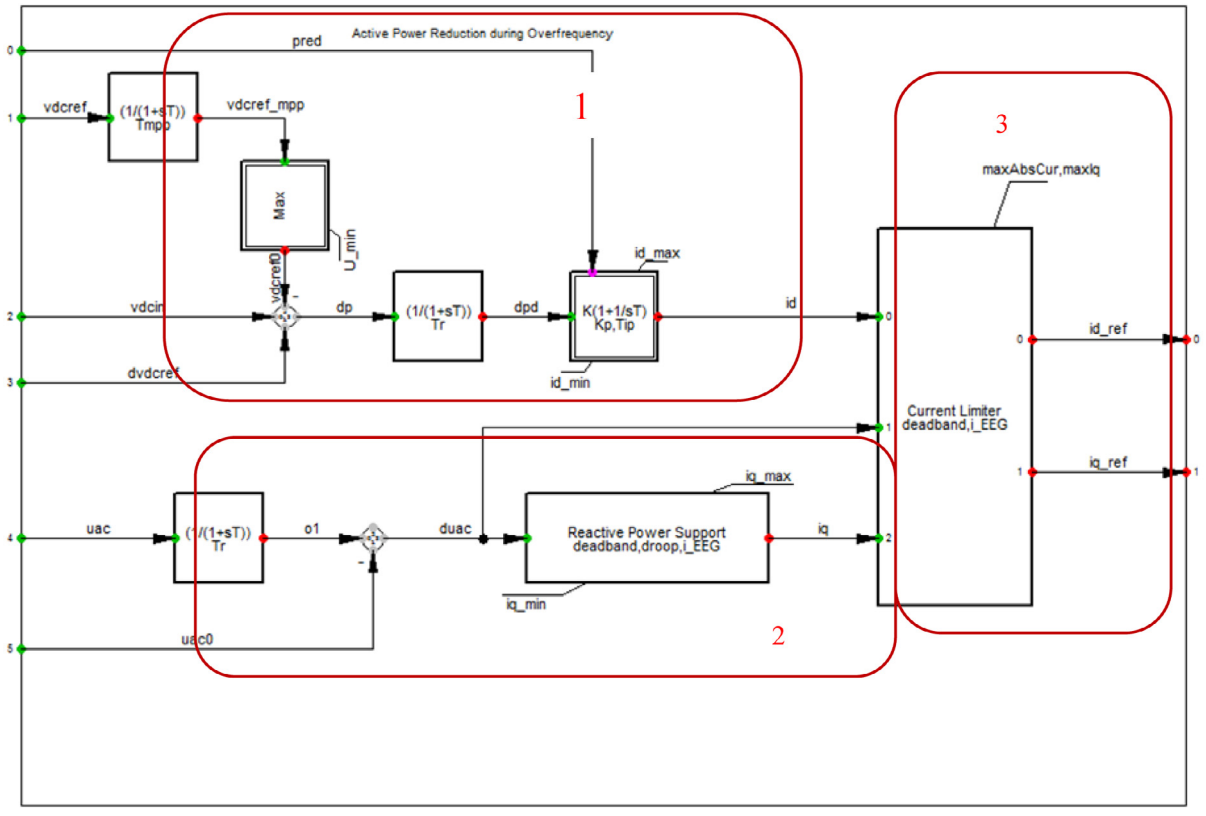

Fig. 28. Solar farm controller model.

Table 8
Solar LVRT blocks function description.

Blocks	Blocks name	Input	Output	Function	Remark(s)
Block 1	Solar radiation	Irradiance per second		To accumulate change of irradiance per second and then integrate over a time.	
Block 2	Temperature	Temperature per second		To accumulate change of temperature per second and then integrate over a time.	
Block 3	Photovoltaic model	Irradiation, Temperature and DC Voltage	Generate array current and reference DC Voltage	Depending on PV array, it is used to calculate PV array current and DC voltage.	No MPPT controller is designed in the PV model, with the help of approximations and assumptions, maximum point is achieved.
Block 4	DC Busbar and capacitor	Array current and active power signal	DC link voltage	DC link voltage across the capacitor is calculated	Dynamic behaviour of the capacitor is included.
Block 5	Controller	DC voltage from capacitor and PV model, active power and AC measure voltage	d-axis current component i_d (for active power) and q-axis current component i_q (for reactive power)	Active–reactive power are regulated	
Block 6	Static Generator	Currents i.e. i_d and i_q		It controls the negative sequence current.	

microgrid, primarily differentiated on time horizon. The normal transient faults generally required LVRT applicability 150–300 ms, whereas grid transformation into multi clusters with integrated DERs may require up to 650 ms to become stable due to switching operations of smart switches (sectionalizer). Therefore, controller can differentiate the event phenomena and consequently can generate the report.

6. LVRT visibility in resiliency enhancement — A case study

In the last decade, the electrical distribution grid has seen much destruction due to high impact natural calamity. As per the Indian case study, the last five years have witnessed many-fold increase in high-impact natural calamities. Moreover, it is essential to serve critical loads such as hospitals during the pandemic. Fortunately, no natural calamity occurred during the crucial period of the pandemic; otherwise, it could have been devastating. Therefore, a resilient distribution grid is necessary for the future. Numerous techniques have been proposed in the literature for enhancing electrical grid resilience. However, the need for LVRT during the transformation from one grid to many clustered grids during natural disasters has been overlooked in the literature. To demonstrate the need for LVRT in the distribution grid, we performed an electrical grid distribution simulation of an urban city in India using the PowerFactory software.

To validate the requirement of LVRT, authors have used urban distribution grid (Uttarakhand, India) data and simulated it on the DIgSILENT PowerFactory. The significance of the study region is that it lies in an extreme seismic zone, and more than 60% of the geographical features are covered by Himalayan Hill's range. Therefore, based on the historical catalogue, the probability of earthquakes and subsequent landslides places the region in a highly prone area. Moreover, the considered regions account for tourist attractions from all over India and internationally due to Himalayan range and wild life along with the widely popular religious fair, "Kumbh", which happens every five years.

In contrast, the simulated electrical distribution grid of the region consisted of 156 buses of 33 kV and 11 kV along with six grid-integrated solar PV plants by utility. Geographical features, along with social and touristic aspects, make the entire distribution grid vulnerable. However, the preliminary planning actions for resilient electrical grids (Nasri et al., 2022), can enable the system to fulfil the critical demand during any adverse event. In addition, the transition of the grid from the normal mode to the survival mode also requires LVRT.

Therefore, to observe the change during grid transformation, quasi-dynamic load flow was performed on a simulated grid for 24-h time with a step size of 15 min under normal conditions. The heat map and voltage profile variations are shown in Fig. 29 and Table 7, respectively.

The second simulation was conducted after considering the vulnerability effects of natural disasters (earthquakes) on an electrical distribution grid (Yadav et al., 2021). Moreover, this article considers the line state, "damage" if the probability of damage is more than 60% duly considering fragility curve (Johnson et al., 2020). Henceforth, grid transformation has been performed after omitting the vulnerable lines and only considering already defined critical loads such as hospitals, COVID wards, water pump houses, and communication centres. The procedure for determining the damage probability of each line is presented as a flowchart in Fig. 30.

To modelled the impact of earthquake a data sample has been created from the historical catalogue of earthquake occurred in the study region (Discovery, 2022). This data sample have been used to formulate probability distribution function (PDF) for location and magnitude, represented in Eqs. (3) & (4).

$$PDF_{Location}\,(L_c) = \frac{1}{\sqrt{(2\pi)}\sigma[L_c]} \times e^{-\left(L_c - \mathrm{E}(L_c)/\sqrt{2}\sigma[L_c]\right)^2} \tag{3}$$

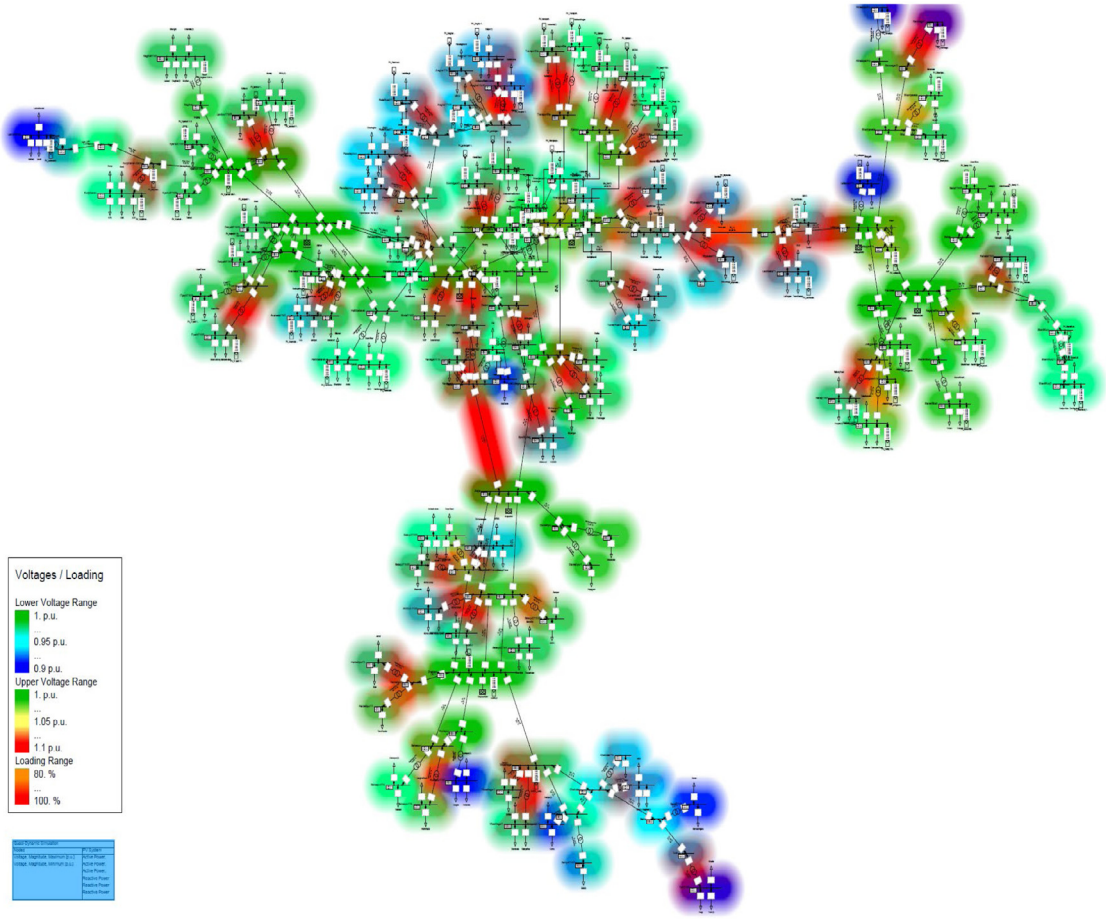

Fig. 29. Heatmap of case study (Dehradun grid) after quasi-dynamic load flow.

$$PDF_{Magnitude}\,(M_{eh}) = \frac{1}{\sqrt{(2\pi)}\sigma\,[M_{eh}]} \times e^{-\left(M_{eh}-\mathrm{E}(M_{eh})/\sqrt{2}\sigma\,[M_{eh}]\right)^2} \quad (4)$$

Therefrom, authors have identified probabilistic occurrence of earthquake in future and located the severe most earthquake occurrence near or within study zone. The peak ground acceleration (PGA, Eq. (5)) (Liu et al., 2003) for each selected earthquake have been formulated to classify the damage probability in four categories, "safe", "slight", "50-50", "certain", after superimposing the fragility curves of distribution lines (Eq. (6)).

$$PGA = 0.02938e^{1.19950(M_{eh})} * \left[R + 0.14667e^{0.69689(M_{eh})}\right]^{-1.73413} \quad (5)$$

where, M_{eh} is earthquake magnitude and R is radial distance between fault earthquake line and site.

$$F\,(x) = \frac{1}{2}\left[1 + erf\left(\frac{\ln\,(x) - \mu}{\sigma\sqrt{2}}\right)\right] \quad (6)$$

where, (x) = Random variable, μ = mean, σ = standard deviation.

x is taken from standard normal random variable Z.

Fig. 31 shows the heat map, which clearly indicates that some of the zones are in the dark, and a few of the transformers are overloaded. Table 9 shows the deliberate voltage variability (min, max) after disaster transformation. During an event (high impact low probability), when grid transform into several clusters then voltage profile of each clusters also changes. This substantiates the requirement of voltage ride through capability for the transformation of one grid into several clusters with updated settings and logic to enhance the resiliency

7. Discussion

The paper discusses the impact of increasing influx RES and EVs into the low-voltage distribution grid and the various grid codes adopted by different countries. Furtherance to distributed energy generation, stochastic load demand burdened by EVs, and increasing natural calamities dictates the need of resilient power system network. Therefore, this paper also discusses the requirement of low-voltage ride through in the grid code while integrating RES into the distribution grid. The above work also shows the results that reflects the importance of voltage ride through capability to make the distribution grid more resilient to natural disasters. It has also been shown that the grid voltage and frequency vary from the normal mode to the transformation mode of the grid while changing its state during the disaster. This article covers the factors related to the LVRT. In addition, after showing the importance of the LVRT for resiliency enhancement, various controller techniques available for the enhancement of LVRT requirements for grid integration of solar and wind were well presented in Section 5. For a clearer understanding, this paper describes the implementation of LVRT by taking the example of the DIgSILENT PowerFactory software by considering six wind turbines and a 20 kV external grid. It was found that the implementation of LVRT in a wind-integrated distribution grid is more complex than that of a solar PV plant. As the wind power plant has a rotatory machine and for the implementation of LVRT, we need to control the inertia or rotation of the machine, whereas the solar PV plant has been considered as a static generator. For the LVRT implementation, the controller for the control mechanism is less tedious compared to the wind power plant. It is evident that,

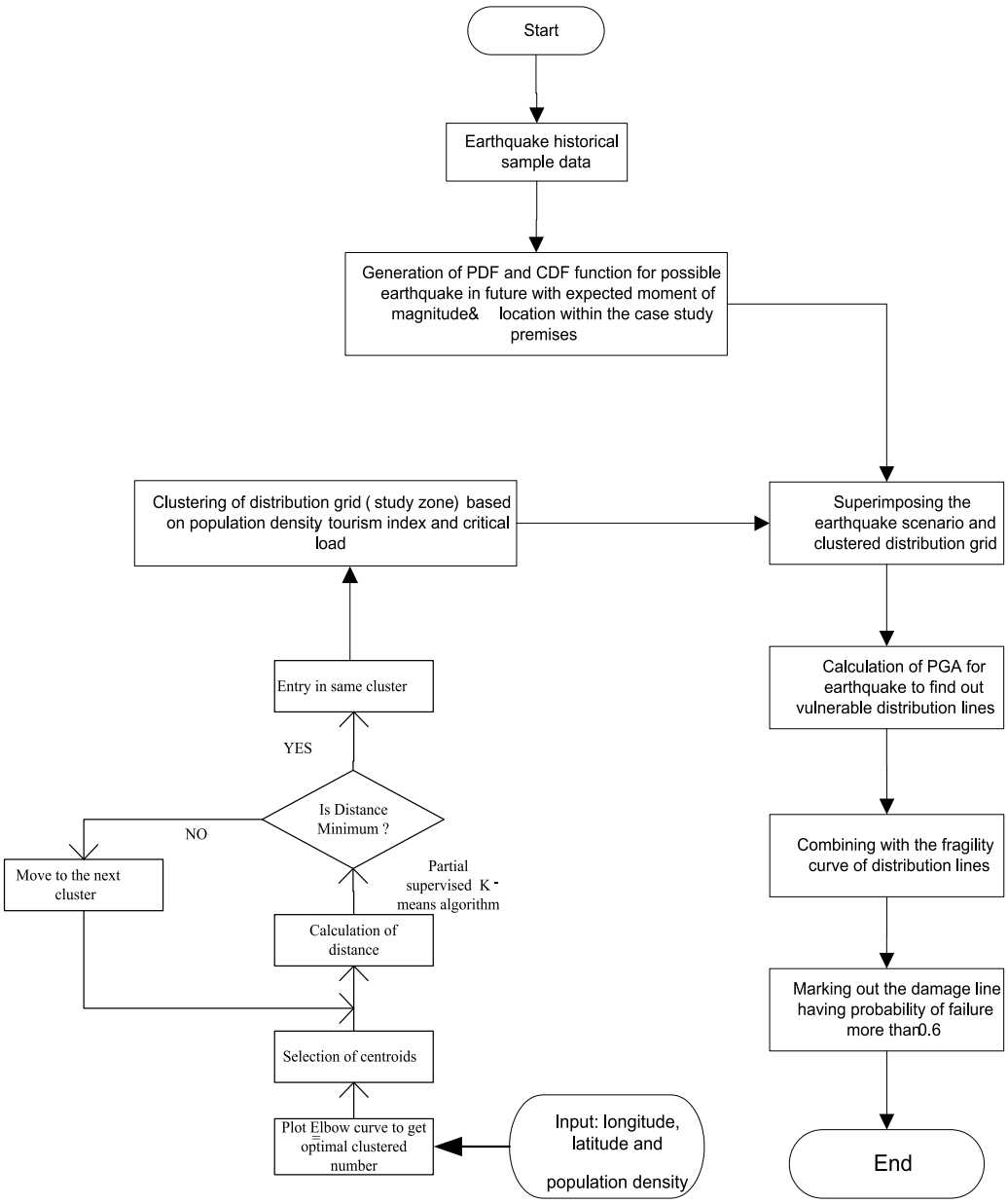

Fig. 30. Flowchart to modelled earthquake & identify vulnerable distribution line.

Table 9
Voltage profile variation.

S. No	Bus location(s)		Voltage profile before the event		Voltage profile after the event	
	Latitude	Longitude	Vmax	Vmin	Vmax	Vmin
1	30.3069	78.0499	0.94	0.93	0.89	0.84
2	30.3136	78.04045	0.96	0.94	0.88	0.86
3	30.3245	78.0484	0.95	0.94	0.89	0.87
4	30.3035	78.1046	0.97	0.96	0.91	0.9
5	30.38723	78.13161	0.98	0.97	0.96	0.95
6	30.348	78.0523	0.98	0.97	0.97	0.96
7	30.3266	78.0357	0.98	0.96	0.99	0.98
8	30.267	78.0909	0.99	0.99	1	0.99
9	30.3226	78.0037	0.98	0.98	0.89	0.88
10	30.3306	77.9574	1	0.99	0.94	0.93
11	30.3518	78.0095	0.98	0.97	1	0.98
12	30.3927	77.8096	0.98	0.97	0.99	0.97
13	30.4383	77.736	0.99	0.97	0.98	0.97
14	30.3572	78.087	0.97	0.96	0.97	0.96

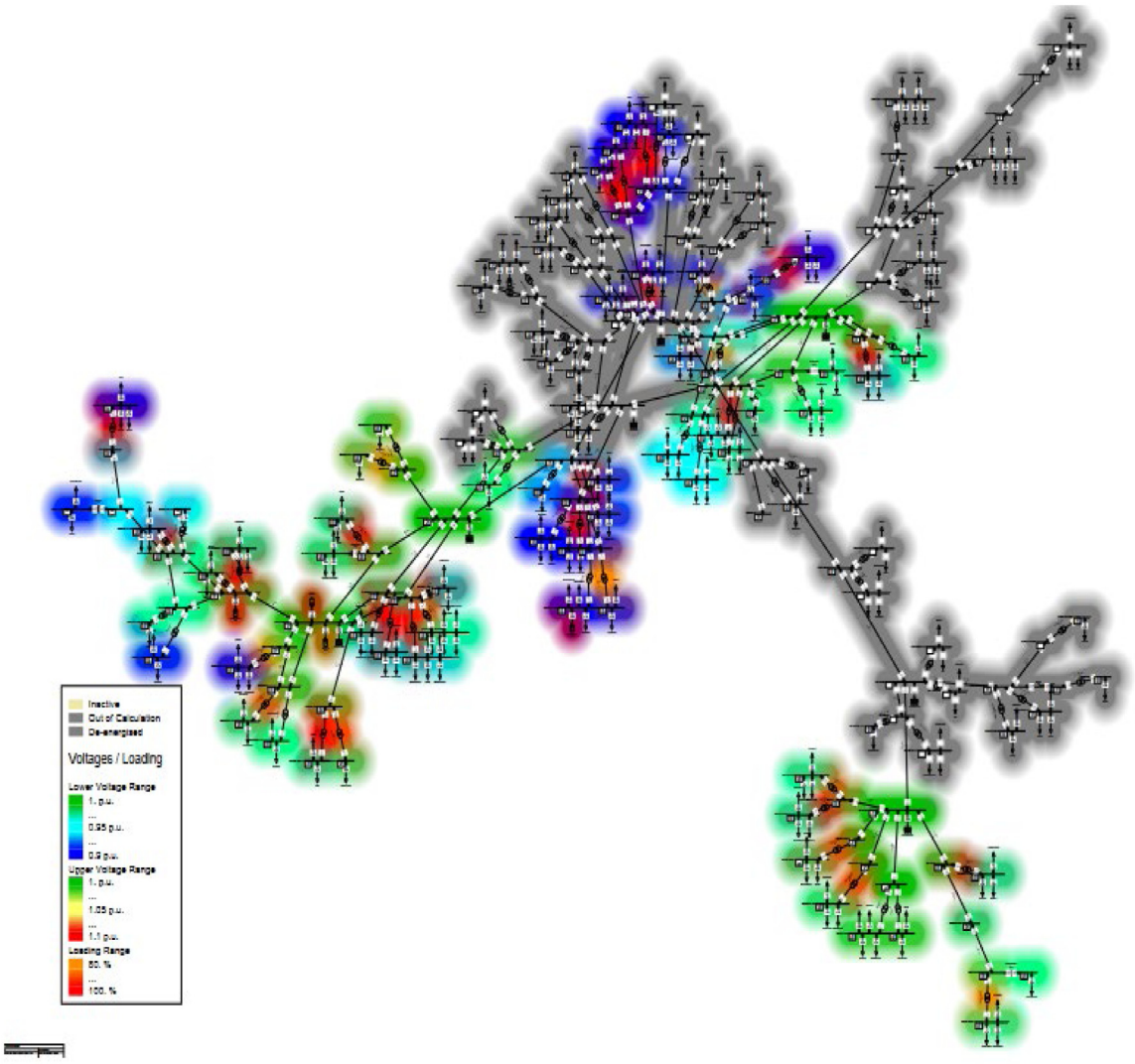

Fig. 31. Heatmap of Dehradun grid with damage line.

to make the RES connected distribution grid more resilient, the LVRT requirement must be implemented, though most countries have developed their grid codes by considering LVRT. However, a robust grid code and policy are still required to implement precise control strategies for LVRT when we create a resilient distribution system against natural disasters such as earthquakes, landslides, floods, and cloudbursts. Hence, it is proposed that a new LVRT requirement, which can be generalized for the normal operating mode of the grid and the transformation mode of the grid during a disaster, needs to be implemented.

8. Conclusion

This study mainly focuses on the importance of low-voltage ride through in a distribution grid. The deployment of RES in the grid has increased and will continue to grow to meet the rising demand. This shows that the sudden disconnection of renewable sources from the grid causes numerous problems. Therefore, a LVRT requirement for RES is required. This study presents a comprehensive review of grid code requirements followed by different countries for the deployment of RES into the grid. In addition, a detailed analysis of the IEEE 1547 standards and reactive current support for the grid voltage is presented.

The LVRT capability works with the help of the controller mechanism. Moreover, various control strategies for the enhancement of LVRT capability in solar and wind power are presented. The literature on LVRT grid code in PV-connected systems revealed that an efficient DC link voltage control method is required. The simulation results have been obtained after creating a fault at PCC with two scenarios. The results show that the behaviour of the grid voltage is comparable, and it is clearly visible that with the inclusion of the fault impedance, the grid voltage does not collapse to zero, and the reactive power is higher than the active power.

Moreover, the study performed a simulation on a real distribution grid with 156 buses integrated with six PV systems. To observe the change during grid transformation, a quasi-dynamic load flow was performed. The maximum likelihood estimation has been implemented to draw the fragility curve of feeders and presented as a flowchart. Henceforth, grid transformation has been performed after omitting the vulnerable lines and only considering already defined critical loads. The simulation results

show the voltage variability before and after the event. Hence, it is concluded that during grid transformation, voltage ride through capabilities with updated settings and logic are required to enhance resiliency in operational methods.

Declaration of competing interest

The authors declare that they have no known competing financial interests or personal relationships that could have appeared to influence the work reported in this paper.

Data availability

The data set e.g. distribution grid's line and loading, tourism index of taken case study, population density, and earthquake profile to generate PDF functions, used in this paper can be found at: https://drive.google.com/drive/folders/1hjhM1VAgIcjZlsT0466AdV7y-quRNkQB?usp=sharing.

Acknowledgement

Authors would to thank DigSILENT Power factory, Germany for providing software licence for this research under PF4T scheme.

References

Abulanwar, E.S.M., 2016. Wind power integration into weak power systems.
Ahmad, T., Madonski, R., Zhang, D., Huang, C., Mujeeb, A., 2022. Data-driven probabilistic machine learning in sustainable smart energy/smart energy systems: Key developments, challenges, and future research opportunities in the context of smart grid paradigm. Renew. Sustain. Energy Rev. 160 (January), 112128. http://dx.doi.org/10.1016/j.rser.2022.112128.
Amalorpavaraj, R., Natarajan, P., El-Moursi, M., Rosen, M.A., Kaliannan, U., Subramaniam, P., 2020. An outlook on endangering grid security in India due to implementation challenges of low voltage ride through protection in wind turbines. Int. Trans. Electr. Energy Syst. 30 (12).
Bahramian-Habil, H., Askarian Abyaneh, H., Gharehpetian, G.B., 2021. Improving LVRT capability of microgrid by using bridge-type fault current limiter. Electr. Power Syst. Res. 191.
Basso, T., 2014. IEEE 1547 and 2030 Standards for Distributed Energy Resources Interconnection and Interoperability with the Electricity Grid IEEE 1547 and 2030 Standards for Distributed Energy Resources Interconnection and Interoperability with the Electricity Grid, Vol. December. Nrel, p. 22.
2007. BDEW Shichao Generating Plants Connected To the Medium-Voltage Network (Guideline for Generating Plants' Connection To and Parallel Operation with the Medium-Voltage Network) BDEW. Germany.
Benyamina, F., Benrabah, A., Khoucha, F., Fahad, M., Achour, Y., Benbouzid, M., 2021. Online current limiting-based control to improve fault ride-through capability of grid-feeding inverters. Electr. Power Syst. Res. 201 (June), 107524.
Cabrera-Tobar, A., Bullich-Massagué, O., Aragüés-Peñalba, E., Gomis-Bellmunt, M., 2016. Review of advanced grid requirements for the integration of large scale photovoltaic power plants in the transmission system. Renew. Sustain. Energy Rev. 62, 971–987.
Das, L., Munikoti, S., Natarajan, B., Srinivasan, B., 2020. Measuring smart grid resilience: Methods, challenges and opportunities. Renew. Sustain. Energy Rev. 130 (June), 109918.
DIgSILENT, 2022. DIgSILENT power factory. [Online]. Available: www.digsilent.de.
Ding, T., Lin, Y., Bie, Z., Chen, C., 2017. A resilient microgrid formation strategy for load restoration considering master–slave distributed generators and topology reconfiguration. Appl. Energy 199, 205–216.
Ding, Tao, Qu, Ming, Wang, Zekai, Chen, Bo, Chen, Chen, Shahidehpour, Mohammad, 2020. Power system resilience enhancement in typhoons using a three-stage day-ahead unit commitment. IEEE Trans. Smart Grid 12 (3), 2153–2164.
Discovery, V., 2022. VolcanoDiscovery. [Online]. Available: https://www.volcanodiscovery.com/home.html.
Duong, M.Q., Leva, S., Mussetta, M., Le, K.H., 2018. A comparative study on controllers for improving transient stability of DFIG wind turbines during large disturbances. Energies 11 (3).
ECM, E.C.M., 2017. Grid code for peninsular Malaysia.
Eirgrid, 2015. Eirgrid grid code - version 6.0.
2006. E.on Netz Shichao Grid Code High and Extra High Voltage E.on Netz GmbH. Bayreuth, Germany.
Erlich, J.J., Istvan, Korai, Abdul, Neumann, Tobias, Zadeh, Masoumeh Koochack, Vogt, Steffen, Buchhagen, Christoph, Rauscher, Cristian, Menze, Andreas, 2017. New control of wind turbines ensuring stable and secure operation following islanding of wind farms. IEEE Trans. Energy Convers. 32 (3), 1263–1271.
2009. ES-AENOR Shichao Wind Turbines – Part 21: Measurement and Assessment of Power Quality Characteristics of Grid Connected Wind Turbines (UNE-EN 61400-21-2009) AENOR. Spanish.
Etxegarai, A., Eguia, P., Torres, E., Iturregi, A., Valverde, V., 2015. Review of grid connection requirements for generation assets in weak power grids.. Renew. Sustain. Energy Rev. 41, 1501–1514.
European Committee for Electrotechnical Standardization, 2015. Requirements for micro-generating plants to be connected in parallel with public low-voltage distribution networks.
Feng, Z., Joyce, L., Alyssa, P., 2021. Global wind report 2021.
Firouzi, M., Gharehpetian, G.B., 2018. LVRT performance enhancement of DFIG-based wind farms by capacitive bridge-type fault current limiter. IEEE Trans. Sustain. 9 (3), 1118–1125.
Fu, R., Feldman, D.J., Margolis, R.M., 2018. US Solar Photovoltaic System Cost Benchmark: Q1 2018. Natl. Renew. Energy Lab.(NREL), Golden, CO (United States).
Gao, H., Chen, Y., Xu, Y., Liu, C.-C., 2016. Resilience-oriented critical load restoration using microgrids in distribution systems. IEEE Trans. Smart Grid 7 (6), 2837–2848.
Gholizadeh, Mahyar, Oraee, Ashknaz, Tohidi, Sajjad, Oraee, Hashem, McMahon, Richard A., 2018. An analytical study for low voltage ride through of the brushless doubly-fed induction generator during asymmetrical voltage dips. Renew. Energy (ISSN: 0960-1481) 115, 64–75.
Gkavanoudis, S.I., Demoulias, C.S., 2015. A control strategy for enhancing the fault ride- through capability of a microgrid during balanced and unbalanced grid voltage sags. Sustain. Energy Grids Net. 3, 1–11.
Golchoob Firoozjaee, M., Sheikh-El-Eslami, M.K., 2021. A hybrid resilient static power system expansion planning framework. Int. J. Electr. Power Energy Syst. 133.
Gonzalez Venegas, F., Petit, M., Perez, Y., 2020. Active integration of electric vehicles into distribution grids: Barriers and frameworks for flexibility services. Renew. Sustain. Energy Rev. 145, 2021. http://dx.doi.org/10.1016/j.rser.2021.111060.
H, T., Gao, F., Ma, C., He, G., Li, G., 2014. A review of low voltage ride-through techniques for photovoltaic generation systems. In: IEEE Energy Conversion Congress and Exposition. pp. 1566–1572.
Hagh, M.T., Khalili, T., 2019. A review of fault ride through of PV and wind renewable energies in grid codes. Int. J. Energy Res. 43 (4), 1342–1356.
Hansen, A.D., Das, K., Sørensen, P., Singh, P., Gavrilovic, Andrea, 2021. European and Indian grid codes for utility scale hybrid power plants. Energies 14 (14).
Hassan, Z., Amir, A., Selvaraj, J., Rahim, N.A., 2020. A review on current injection techniques for low-voltage ride-through and grid fault conditions in grid-connected photovoltaic system. Sol. Energy 207 (July), 851–873.
Hil, T., 2020. LVRT in generic DER components.
Hiremath, Ravikiran, Moger, Tukaram, 2022. Modified super twisting algorithm based sliding mode control for LVRT enhancement of DFIG driven wind system. Energy Rep. 8, 3600–3613.
Hossain, H.R., Saha, M.J., Mithulananthan, T.K., Pota, N., 2012. Control strategies for augmenting LVRT capability of DFIGs in interconnected power systems. IEEE Trans. Ind. Electron. 60 (6), 2510–2522.
Howlader, A.M., Senjyu, T., 2016. A comprehensive review of low voltage ride through capability strategies for the wind energy conversion systems. Renew. Sustain. Energy Rev. 56, 643–658.
IIT Kanpur, 2001. Gujarat Earthquake. India.
2013. India Raises Flood Death Toll To 5, 700 As All Missing Persons now Presumed Dead. CBS.
Jawad, A., Massod, N.A., 2022. A systematic approach to estimate the frequency support from large-scale PV plants in a renewable integrated grid. Energy Rep. 8, 940–954.
Jerin, R.A., Thomas, A.M., K, P., S, U., 2018. Enhancing low voltage ride through capability in utility grid connected single phase solar photovoltaic system. J. Eng. Sci. Technol. 13 (4), 1016–1033.
Jha, D., 2017. A comprehensive review on wind energy systems for electric power generation: Current situation and improved technologies to realize future development. Int. J. Renew. Energy Res. 7, 41786–41805.
Jian, Wang, Ben, Yue, Zhang, Jinrui, Feng, Hao, 2022. Low voltage ride-through control strategy for a wind turbine with permanent magnet synchronous generator based on operating simultaneously of rotor energy storage and a discharging resistance. Energy Rep. 8, 5861–5870.
Johnson, B., Chalishazar, V., Cotilla-sanchez, E., Brekken, T.K.A., 2020. A Monte Carlo methodology for earthquake impact analysis on the electrical grid. Electr. Power Syst. Res. 184 (2019), 106332.
Joshi, J., Swami, A.K., Jately, V., Azzopardi, B., 2021. A comprehensive review of control strategies to overcome challenges during LVRT in PV systems. IEEE Access 9, 121804–121834.

Karaağaç, D., 2020. Generator types used in wind turbines. [Online]. Available: http://dx.doi.org/10.13140/RG.2.2.10717.64488.
Kasem, M.A.A., A.H. El-Saadany, E.F. El-Tamaly, Wahab, H.H., 2018. An improved fault ride-through strategy for doubly fed induction generator-based wind turbines. IET Renew. Power Gener. 2 (4), 201–214.
Kekatos, V., Zhang, L., Giannakis, G.B., Baldick, R., 2015. Voltage regulation algorithms for multiphase power distribution grids. IEEE Trans. Power Syst. 31 (5), 3913–3923.
Lamnatou, Chr., Chemisana, D., Cristofari, C., 2022. Smart grids and smart technologies in relation to photovoltaics,storage systems, buildings and the environment. Renew. Energy 185, 1376–1391.
Li, Tiecheng, Fan, Hui, Zeng, Siming, Hu, Xuekai, Meng, Zhengji, Zhao, Yuhao, 2022. A low voltage ride-through strategy for grid-connected PV converters based on variable power point tracking method. Energy Rep. 8, 398–404.
Li, Fei, Liu, Mengtao, Wang, Yingfeng, Zhang, Xing, 2021. Research on HIL-based HVRT and LVRT automated test system for photovoltaic inverters. Energy Rep. 7, 405–412.
Liu, G.-Y., Liu, C.-Y., Wang, Y.-J., 2003. Monte Carlo simulation for the seismic response analysis of electric power system in Taiwan. In: NCREE/JRC Jt. Work.
Lokesh, M., Kulkarni, N., Ananthapadmanabha, A.D., Gurav, T., Kumar, K.S., 2021. Enhancement of transient stability and voltage quality of microgrid with multiple DERs. In: 2021 5th International Conference on Intelligent Computing and Control Systems. ICICCS, pp. 686–691.
Mahmood, F., 2012. Improving the photovoltaic model in PowerFactory.
Mali, I., James, S., Tank, S., 2014. Improving low voltage ride-through capabilities for grid connected wind turbine generator. Energy Procedia 54, 530–540.
Manikanta, B., Kesavarao, G., Talati, S., 2017. LVRT of grid connected PV system with energy storage. Int. Sci. Press 10 (5), 75–86.
Mishra, D.K., Ghadi, M.J., Azizivahed, A., Li, L., Zhang, J., 2020. A review on resilience studies in active distribution systems. Renew. Sustain. Energy Rev. 135, 2021.
Moghadasi, A., Sarwat, A., Guerrero, J.M., 2016. A comprehensive review of low-voltage-ride-through methods for fixed-speed wind power generators. Renew. Sustain. Energy Rev. 55, 823–839.
Muaelou, H., Badran, E.A., Abo-Al-Ez, K.M., 2016. A proposed control strategy for low voltage ride through capability of PV system with keeping the DC-link voltage constant. J. Electr. Eng. 16 (2).
Muyeen, J., Takahashi, S.M., Murata, R., Tamura, T., 2009. A variable speed wind turbine control strategy to meet wind farm grid code requirements. IEEE Trans. Power Syst. 25 (1), 331–340.
Nasiri, M., Arzani, A., McCormack, S.J., 2022. A simple and effective grid-supporting low voltage ride-through scheme for single-stage photovoltaic power plants. Sol. Energy 232, 248–262.
Nasri, A., Abdollahi, A., Rashidinejad, M., 2022. Multi-stage and resilience-based distribution network expansion planning against hurricanes based on vulnerability and resiliency metrics. Int. J. Electr. Power Energy Syst. 136.
Nivedh, B.S., Tentzerakis, S., Dirksen, J., Santjer, F., 2017. Testing procedure for the evaluation of grid compliance of power generating units according to the requirements of the Indian Grid Code. In: Re Grid Integration.
Oh, Seongmun, Jufri, Fauzan Hanif, Choi, Min-Hee, Jung, Jaesung, 2022. A study of tropical cyclone impact on the power distribution grid in South Korea for estimating damage. Renew. Sustain. Energy Rev. 156, 112010.
Oon, K.H., Tan, C.K., Bakar, A.H.A., Che, H.S., Mokhlis, H., Illias, H.A., 2018. Establishment of fault current characteristics for solar photovoltaic generator considering low voltage ride through and reactive current injection requirement. Renew. Sustain. Energy Rev. 92 (May), 478–488.
Pal, D., Panigrahi, B.K., 2020. Analysis and mitigation of the impact of ancillary services on anti-islanding protection of distributed generators. IEEE Trans. Sustain. Energy 11 (4), 2950–2961.
Panteli, Mathaios, Trakas, Dimitris N., Mancarella, Pierluigi, Hatziargyriou, Nikos D., 2016. Boosting the power grid resilience to extreme weather events using defensive islanding. IEEE Trans. Smart Grid 7 (6), 2913–2922.
Parvez, M., Elias, M.F.M., Rahim, N.A., Osman, N., 2016. Current control techniques for three-phase grid interconnection of renewable power generation systems: A review. Sol. Energy 135, 29–42.
Paul, D.K., Singh, Yogendra, Dubey, R.N., 2018. Damage To Andaman & Nicobar Islands Due To Earthquake and Tsunami of Dec. 26, 2004. PDF, Department of Earthquake Engineering, IIT Roorkee.
Racy, 2012. Severe Thunderstorm Watch 435. Storm Prediction Center. National Oceanic and Atmospheric Administration.
Rebollal, D., Carpintero-Rentería, M., Santos-Martín, D., Chinchilla, M., 2021. Microgrid and distributed energy resources standards and guidelines review: Grid connection and operation technical requirements. Energies 14 (3).
Redlinger, P., Andersen, R., Morthorst, P., 2016. Wind Energy in the 21st Century: Economics, Policy, Technology and the Changing Electricity Industry. Springer. Springer.
Rocchetta, R., 2022. Enhancing the resilience of critical infrastructures: Statistical analysis of power grid spectral clustering and post-contingency vulnerability metrics. Renew. Sustain. Energy Rev. 159 (January).
Saad, Naggar H., El-Sattar, Ahmed A., Mansour, Abd El-Aziz M., 2016. Improved particle swarm optimization for photovoltaic system connected to the grid with low voltage ride through capability. Renew. Energy (ISSN: 0960-1481) 85, 181–194.
Sadeghkhani, I., Hamedani Golshan, M.E., Mehrizi-Sani, A., Guerrero, J.M., 2018. Low- voltage ride-through of a droop-based three-phase four-wire grid-connected microgrid. IET Gener. Transm. Distrib. 12 (4), 1906–1914.
Sepúlveda-Mora, Sergio B., Hegedus, Steven, 2022. Resilience analysis of renewable microgrids for commercial buildings with different usage patterns and weather conditions. Renew. Energy (ISSN: 0960-1481) 192, 731–744.
Shabestary, M.M., Mohamed, Y.A.-R.I., 2020. Autonomous coordinated control scheme for cooperative asymmetric low-voltage ride-through and grid support in active distribution networks with multiple DG units. IEEE Trans. Smart Grid 11 (3), 2125–2139.
Sourkounis, C., Tourou, P., 2013. Grid code requirements for wind power integration in Europe. Conf. Pap. Energy 2013, 1–9.
Talha, Muhammad, Raihan, S.R.S., Abd Rahim, N., 2020. PV inverter with decoupled active and reactive power control to mitigate grid faults. Renew. Energy (ISSN: 0960-1481) 162, 877–892.
Tan, A., Tang, Z., Sun, X., Zhong, J., Liao, H., Fang, H., 2020. A cut-out strategy for wind turbines that ensures low-voltage ride-through capability. J. Electr. Eng. Technol. 15 (4), 1567–1575.
Tsili, S., Papathanassiou, M., 2009. A review of grid code technical requirements for wind farms. IET Renew. Power Gener. 3 (3), 308–332.
U.S.D. of Energy, 2021. International energy outlook 2021 narrative.
Venkateswaran, V.B., Saini, D.K., Sharma, M., 2020. Approaches for optimal planning of energy storage units in distribution network and their impacts on system resiliency. CSEE J. Power Energy Syst. 6 (4), 816–833. http://dx.doi.org/10.17775/CSEEJPES.2019.01280.
Ward, D.J., 2001. Power quality and the security of electricity supply. Proc. IEEE 89 (12), 1830–1836.
2005. Western Electricity Coordination Council (WECC) Shichao Low Voltage Ride Through Standard WECC. New York, USA.
Xu, Y., Liu, C.-C., Schneider, K.P., Tuffner, F.K., Ton, D.T., 2016. Microgrids for service restoration to critical load in a resilient distribution system. IEEE Trans. Smart Grid 9 (1), 426–437.
Xue, J., 2017. Photovoltaic agriculture-new opportunity for photovoltaic applications in China. Renew. Sustain. Energy Rev. 73, 1–9.
Yadav, M., Pal, N., Saini, D.K., 2020. Microgrid control, storage, and communication strategies to enhance resiliency for survival of critical load. IEEE Access 8, 169047–169069.
Yadav, M., Pal, N., Saini, D., 2021. Resilient electrical distribution grid planning against seismic waves using distributed energy resources and sectionalizers: An Indian's urban grid case study. Renew. Energy 178, 241–259.
Yadav, M., Saini, D.K., Pal, N., 2017. Review and compliances of grid code with renewable energy (RE) integration. In: Proc. Int. Conf. Large Scale Grid Integr. Renew. Energy India. pp. 1–9.
Yin, J., Xu, R., 2014. Photovoltaic inverter with control for performing low voltage ride through.
Yongning, C., Yan, L., Zhen, L., Ziyu, C., Hongzhi, L., 2019. Study on grid-connected renewable energy grid code compliance. In: 2019 IEEE Sustainable Power and Energy Conference. ISPEC, pp. 72–75.
Younesi, A., Shayeghi, H., Wang, Z., Siano, P., Mehrizi-Sani, A., Safari, A., 2022. Trends in modern power systems resilience: State-of-the-art review. Renew. Sustain. Energy Rev. 162 (March), 112397.
Yuan, X., Tan, Z., Weng, H., 2013. Apparatus and method for DC/AC systems to ride through grid4. Transients.
Zhao, X., Guerrero, J.M., Savaghebi, M., Vasquez, J.C., Wu, X., Sun, K., 2017. Low-voltage ride-through operation of power converters in grid-interactive microgrids by using negative-sequence droop control. IEEE Trans. Power Electron. 32 (4), 3128–3142.
Zhou, J., Zhou, H., Qi, Z., No TitleZhou, J., Zhou, H., Qi, Z., 2008. The study on a dual-feed-forward control of DVR to mitigate the impact of voltage sags caused by induction motor starting. In: In 2008 International Conference on Electrical Machines and Systems. pp. 1497–1500.

Monika Yadav received her Post-Graduation degree in Electrical Engineering specialization in power system in 2015 from IIT (Indian School Of Mines), Dhanbad - 826004, Jharkhand, India.; also pursuing her Ph.D. in Power System Engineering from IIT (Indian School Of Mines), Dhanbad, India. She has more than 7 yrs. of teaching experience from University of petroleum and energy studies, Dehradun. In addition, she is a certified distribution engineer trainer from power sector skill council of India (PSSC) and ministry of human resources and development (MHRD), India.

Dr. Nitai Pal is currently working as an Associate Professor in the Department of Electrical Engineering, Indian Institute of Technology (ISM), Dhanbad, Jharkhand, India. He has received his B.Tech. and M.Tech. degrees from University of Calcutta, Calcutta, India in 1998 and 2000 respectively. He did his Ph.D. (Engineering) from Jadavpur University, Kolkata, India in the year 2007. He has total experience of 21 years in teaching and research. He has published more than 75 research articles in various international and national journals of repute. Recently, Dr. Pal has successfully completed UGC funded, "Development of Hybrid Off-grid Power Supply System for Remote Areas" research project as PI. Presently, he is involved in various R&D projects under diverse research scheme. He is the member of various professional bodies like: Senior Member IEEE, Member PES (IEEE), Member PELS (IEEE), FIE, IAENG, IACSIT, IDES, IAES, IIIE, ISTE, SSI. His research interests include power electronics applications, power quality, application of high frequency converter, renewable energy & its application, energy efficient devices, energy efficient drives, computer aided power system analysis, condition monitoring, lighting and communication systems for mines etc.

Devender Kumar Saini presently works as Associate Prof. Electrical cluster, school of Engineering, University of Petroleum & Energy Studies, Dehradun, India. He has received his M.Tech. and Ph.D. degrees from IIT Roorkee in 2009 and 2013, respectively. He has done his Ph.D. on controller design for uncertain interval systems and their order reduction. Currently, he is working on protection for integration of renewable energy sources with distribution grid. His areas of interest are fault detection and protection, traction power system, modelling of uncertain interval systems, robust control and challenges in the integration of RE sources with DT grid.